Weather and Forecasting

Atmospheric River Reconnaissance 2021: A Review

--Manuscript Draft--

Manuscript Number:	
Full Title:	Atmospheric River Reconnaissance 2021: A Review
Article Type:	Article
Corresponding Author:	Alison Cobb Center for Western Weather and Water Extremes, Scripps Institution of Oceanography, UCSD San Diego, California UNITED STATES
Corresponding Author's Institution:	Center for Western Weather and Water Extremes, Scripps Institution of Oceanography, UCSD
First Author:	Alison Cobb
Order of Authors:	Alison Cobb
	F.M. Ralph
	Tallapragada Vijay
	Anna M. Wilson
	Christopher A. Davis
	Luca Delle Monache
	James D. Doyle
	Florian Pappenberger
	Carolyn A. Reynolds
	Aneesh Subramanian
	Peter G. Black
	Forest Cannon
	Chris Castellano
	Jason M. Cordeira
	Jennifer S. Haase
	Chad Hecht
	Brian Kawzenuk
	David A. Lavers
	Michael Murphy
	Jack Parrish
	Ryan Rickert
	Jonathan J. Rutz
	Ryan Torn
	Xingren Wu
	Minghua Zheng
Abstract:	Atmospheric River Reconnaissance (AR Recon) 2021 operated for ten weeks from January 13 th to March 22 nd , with 29 Intensive Observation Periods (IOPs), 45 flights and 1142 successful dropsondes deployed in the northeast Pacific. With the availability of two U.S. Air Force C-130s and one National Oceanic and Atmospheric

	Administration (NOAA) G-IV, six sequences were accomplished, in which the same synoptic system was sampled over several days. Targeted dropsonde observations were focused on essential atmospheric structures, primarily atmospheric rivers. Adjoint and ensemble sensitivities, mainly focusing on predictions of U.S. West Coast precipitation, provided complementary information on locations where additional observations may help to reduce the forecast uncertainty. Additionally, Airborne Radio Occultation (ARO) and tail radar were active during some flights, 30 drifting buoys were distributed, and 111 radiosondes were launched from four locations in California. Dropsonde, radiosonde and buoy data were available for assimilation in real-time into operational models. The principal aim was to gather observations to improve forecasts of landfalling atmospheric rivers on the U.S. West Coast, with the sampling of other meteorological phenomena forecast to have downstream impacts over the U.S. also considered. Alongside forecast improvement, observations were also gathered to address important scientific research questions, as part of a Research and Operations Partnership.
Suggested Reviewers:	Xubin Zeng xubin@arizona.edu
	David Novak david.novak@noaa.gov
	Vanda Grubisic grubisic@ucar.edu

Atmospheric River Reconnaissance 2021: A Review

Alison Cobb[1], F. Martin Ralph[1], Vijay Tallapragada[2], Anna M. Wilson[1], Christopher A. Davis[3], Luca Delle Monache[1], James D. Doyle[4], Florian Pappenberger[5], Carolyn A. Reynolds[4], Aneesh Subramanian[6], Peter G. Black[7], Forest Cannon[1], Chris Castellano[1], Jason M. Cordeira[8], Jennifer S. Haase[1], Chad Hecht[1], Brian Kawzenuk[1], David A. Lavers[5], Michael Murphy[1], Jack Parrish[9], Ryan Rickert[10], Jonathan J. Rutz[11], Ryan Torn[12], Xingren Wu[13], Minghua Zheng[1]

[1] Center for Western Weather and Water Extremes, Scripps Institution of Oceanography, University of California San Diego, La Jolla, California, USA

[2] NOAA/NWS/NCEP/Environmental Modeling Center, College Park, Maryland, USA

[3] National Center for Atmospheric Research, Boulder, Colorado, USA

[4] Naval Research Laboratory, Monterey, California, USA

[5] European Centre for Medium-Range Weather Forecasts (ECMWF), Reading, UK

[6] Department of Atmospheric and Oceanic Sciences, University of Colorado Boulder, Boulder, Colorado, USA

[7] I.M. Systems Group, Inc., College Park, Maryland, USA

[8] Meteorology Program, Plymouth State University, Plymouth, New Hampshire, USA

[9] National Oceanic and Atmospheric Administration's Aircraft Operations Center (AOC), Office of Marine and Aviation Operations, Lakeland, Florida, USA

[10] 53rd Weather Reconnaissance Squadron, United States Air Force

[11] NOAA/NWS/Western Region Headquarters, Salt Lake City, UT, USA

[12] University at Albany, State University of New York, Albany, New York, USA

[13] National Oceanic and Atmospheric Administration/National Centers for Environmental Prediction/Environmental Modeling Center/I. M. Systems Group, College Park, Maryland, USA

Corresponding author: Alison Cobb, accobb@ucsd.edu

Abstract

Atmospheric River Reconnaissance (AR Recon) 2021 operated for ten weeks from January 13th to March 22nd, with 29 Intensive Observation Periods (IOPs), 45 flights and 1142 successful dropsondes deployed in the northeast Pacific. With the availability of two U.S. Air Force C-130s and one National Oceanic and Atmospheric Administration (NOAA) G-IV, six sequences were accomplished, in which the same synoptic system was sampled over several days.

Targeted dropsonde observations were focused on essential atmospheric structures, primarily atmospheric rivers. Adjoint and ensemble sensitivities, mainly focusing on predictions of U.S. West Coast precipitation, provided complementary information on locations where additional observations may help to reduce the forecast uncertainty. Additionally, Airborne Radio Occultation (ARO) and tail radar were active during some flights, 30 drifting buoys were distributed, and 111 radiosondes were launched from four locations in California. Dropsonde, radiosonde and buoy data were available for assimilation in real-time into operational models.

The principal aim was to gather observations to improve forecasts of landfalling atmospheric rivers on the U.S. West Coast, with the sampling of other meteorological phenomena forecast to have downstream impacts over the U.S. also considered. Alongside forecast improvement, observations were also gathered to address important scientific research questions, as part of a Research and Operations Partnership.

Significance Statement

Atmospheric rivers contribute the majority of western U.S. precipitation and are also responsible for damage associated with extreme precipitation. Over the past several years, the Atmospheric River Reconnaissance (AR Recon) observational campaign has collected vast amounts of in situ data sampling atmospheric rivers and their surrounding area. The aim of this paper is to provide details on the research and operational aspects of AR Recon 2021 alongside highlighting the vast quantity of data gathered and presenting some initial research into the dropsonde data collected. This paper details the diverse range of data collected as well as the large spatial coverage over the northeast Pacific and U.S. West Coast. We also show the value in such observational data, which is used to improve weather forecasts in numerous operational modeling systems. This paper provides an overview of this AR Recon 2021 season and raises future research questions, such as exploring further why certain observational data is rejected from the forecast models.

1. Introduction

Atmospheric rivers (ARs) are long narrow corridors of water vapor transport that are responsible for much of the water vapor flux across the mid-latitudes (Zhu & Newell 1998), while over the U.S. West Coast 82% of ARs are associated with an extratropical cyclone (Zhang et al. 2019). Although ARs are a feature in the North Pacific throughout much of the year, there is a seasonal cycle in their spatial distribution, with ARs most frequently impacting the U.S. West Coast during boreal winter (Mundhenk et al. 2016; Gershunov et al. 2017).

Landfalling ARs have both beneficial and negative impacts, providing the majority of western U.S. precipitation (Dettinger et al. 2011), but are also responsible for damage associated with extreme precipitation (Ralph et al. 2006; Lavers et al. 2011; Waliser and Guan 2017; Corringham et al. 2019; Henn et al. 2020). During the U.S. West Coast wet season (November-April), a few intense and long duration ARs can make the difference between drought and wet years (Dettinger et al. 2011; Ralph et al. 2019); therefore, water resource management can be particularly sensitive to AR activity. ARs are defined by integrated vapor transport (IVT), and along with duration, IVT can be used to categorize ARs into different strengths on the AR Scale, with AR 1 as primarily beneficial and becoming increasingly hazardous up to AR 5 (Ralph et al. 2019).

To advance the understanding and prediction of ARs, there have been multiple observational campaigns to collect data in and around these systems. Atmospheric River Reconnaissance (AR Recon) led by the Center for Western Weather and Water Extremes (CW3E operated in the North Pacific in 2016, 2018, 2019, 2020 and 2021 (Ralph et al. 2020), following on from the CalWater program from 2008 to 2015 (Ralph et al. 2016; Cordeira et al. 2017). Starting in 2020, AR Recon has been designated as an "operational" requirement, as directed by the National Winter Season Operations Plan (OFCM2019). AR Recon 2021 spanned 10 weeks from 13 January to 22 March, and contained 29 Intensive Observation Periods (IOPs), an extension of three weeks and an additional 12 IOPs compared to AR Recon 2020.

AR Recon observations aim to fill the observational data gap that exists within ARs in the lower to middle troposphere, due to the degraded quality of satellite radiances in the presence of thick clouds and precipitation (Zheng et al. 2021a). The primary data collected during AR Recon 2021 were from dropsondes, which were deployed by the U.S. Air Force Reserve's 53rd Weather Reconnaissance Squadron (USAF) C-130s and National Oceanic and Atmospheric Administration (NOAA) G-IV aircraft. Field campaign radiosondes were released from four stations along the U.S. West Coast, drifting buoys with surface pressure sensors were distributed in the northeast Pacific, and Airborne Radio Occultation (ARO; Haase et al. 2014) refractivity profiles were gathered on all NOAA G-IV flights. All AR Recon dropsonde, radiosonde, and buoy data were distributed in real-time, when possible, via the World Meteorological Organization's Global Telecommunication System (GTS) (https://www.wmo.int/pages/prog/www/TEM/GTS/) for operational assimilation into numerical weather prediction (NWP) systems.

Although most observations assimilated in NWP systems are from satellites, the positive impact of dropsonde data on AR forecast skill has been demonstrated in several studies (e.g., Stone et al. 2020; Tallapragada et al. 2021; Zheng et al. 2021b), using forecast sensitivity observation impact (FSOI) diagnostics and full data denial experiments. Drifting buoys equipped with barometers make accurate measurements of sea level pressure and have been shown to contribute to marine weather forecast improvement (Centurioni et al. 2017; Ingleby and Isaksen 2018). Since 2019, the deployment of these drifting buoys with barometers over the northeast Pacific, in partnership with NOAA's Global Drifter Program (GDP), has been considered an important component of AR Recon (Ralph et al. 2020). Almost half of global drifting buoys, and 40% in the northeast Pacific region do not have a pressure sensor. Augmented pressure measurements emerged as an additional priority given the positive impact of this data in remote oceanic areas (e.g., Horányi et al. 2017), and Ingleby and Isaksen (2018) recommended that 'more WMO member countries should consider participating in the GDP barometer upgrade program'.

Alongside the improvement of real-time NWP forecasts, the vast observational datasets collected as part of AR Recon also allow for detailed process studies that further the understanding of the physical processes that govern the dynamics of ARs (e.g., Neiman et al. 2017, 2014; Ralph et al. 2017; Cannon et al. 2020; Demirdjian et al. 2020, Norris et al. 2020; Cobb et al. 2021a). Observations of ARs can also be used in model assessment studies, such as examining model biases and forecast model skill (e.g., Lavers et al. 2018, 2020a; Stone et al. 2018), and their fidelity compared to reanalysis products (e.g., Guan et al. 2018; Cobb et al. 2021b). Therefore, AR Recon addresses both operational, real-time forecasting needs, as well as longer-term research goals, working towards a Research and Operations Partnership (Section 1.2.1).

The purpose of this paper is to provide details on the research and operational aspects of AR Recon 2021, including introducing the new concept of an *AR Recon sequence* and describing the current AR Recon mission. This paper details essential atmospheric structures as well as sensitivity tools, both of which are used in identifying observational targets. It also highlights the vast quantity of data gathered, presenting some initial research into the dropsonde data and its assimilation into three operational NWP systems: Global Forecast System (GFS) run at the National Centers for Environmental Prediction (NCEP); NAVy Global Environmental Model (NAVGEM) run at the U.S. Naval Research Laboratory, and the Integrated Forecasting System (IFS) run at European Centre for Medium-Range Weather Forecasts (ECMWF). In Section 2 a meteorological overview of the 2021 AR Recon season is presented, followed by a discussion of the sampling strategy in Section 3. Section 4 details the observational data collected, with Section 5 describing the data assimilated. Sections 6 and 7 present the challenges and summary. Recommendations for future operational seasons is provided in Section 8.

2. AR Recon 2021 meteorology

AR Recon 2021 collected targeted observations of several significant weather events that impacted the U.S. during January–March 2021 (see Supplementary Table 1). During the third week of AR Recon (26^{th} - 29^{th} January, IOPs 3-8), an AR made landfall in California, with some areas in Central California experiencing AR conditions for nearly 48 consecutive hours (AR 2 conditions according to the Ralph et al. 2019 scale). More than 175 mm of precipitation fell in portions of the Sierra Nevada, Central California Coast Ranges, and western Transverse Ranges. Several feet of snow accumulated across the Sierra Nevada, resulting in closures of major highways, and intense rainfall on recent burn scars caused damaging debris flows in Central and Southern California. Soon after, on 31^{st} January, an AR 2 produced significant precipitation in Northern California and Southern Oregon (IOPs 9-11). On 21 February, another AR 2 made landfall over Washington and

Northern Oregon, bringing more than 125 mm of precipitation to the Olympic Peninsula and North Cascades and more than 60 cm of snow in the higher elevations of the Washington Cascades and Bitterroot Mountains (IOPs 14-16). The combination of near-saturated soil conditions, heavy rain, and melting snow produced minor flooding in Western Washington. During 8th -12th March 2021 (IOPs 22-25), a cutoff low formed over the northeast Pacific and moved southeastward along the U.S. West Coast, bringing light to moderate precipitation to much of California. A lee cyclone formed downstream of the upper-level low, with a region of enhanced poleward moisture transport in the warm sector that interacted with a strengthening baroclinic zone to produce severe weather in the Texas Panhandle, heavy rain and flooding in parts of Kansas and Nebraska, and heavy snow in Colorado and Wyoming on 13th -14th March.

Despite the occurrence of several landfalling ARs over the season, the U.S. West Coast continued to experience abnormally dry to exceptional drought conditions (National Drought Mitigation Center, 2021) that preceded the significant wildfire activity in summer 2021 (Predictive Services National Interagency Fire Center, 2021). Persistent ridging over the northeast Pacific contributed to these abnormally dry conditions, as this synoptic pattern plays a dominant role in deflecting the location of landfalling ARs and hence precipitation (Gibson et al. 2020). The presence of these drought conditions and the considerable contribution of individual ARs to season precipitation totals highlights the beneficial impacts of ARs, as an important supplier of water resources for the U.S. West Coast and a vital part of the climate.

3. AR Recon 2021 sampling strategy

The primary goal of AR Recon is to improve forecasts of the landfall and impacts of ARs on the U.S. West Coast at lead times of 1-5 days, optimizing water management and hazard mitigation strategies (Ralph et al. 2020). This goal is achieved by the assimilation of targeted observational data into forecast models to improve the initial conditions. There are several different targeting methods used during field campaigns, summarized in the review article by Majumdar (2016), and in AR Recon we focus on sampling essential atmospheric structures (Section 3.3) and regions of high forecast sensitivity (Section 3.4).

The sampling strategy of AR Recon 2021 is exemplified in this paper using IOP 7, which sampled the high-impact AR that made landfall in California during 26th –29th January and produced heavy precipitation and damaging debris flows in central and Southern California (Section 2). This IOP deployed both the USAF C-130 and NOAA G-IV aircraft and had high forecast sensitivity (see Table S1, Section 3.4).

As well as analyzing the meteorological features present, it was vital to understand the potential impacts associated with a landfalling event. Key forecast impacts were assessed using AR Recon tools developed at CW3E, such as the landfall tool (Cordeira and Ralph 2021), AR Scale forecast (Ralph et al. 2019), and watershed precipitation forecasts, all available at https://cw3e.ucsd.edu. These first two tools focus on the primary AR metric, IVT, and the watershed forecast was used for a more detailed examination of local-scale precipitation, which provides more information on the potential impacts.

3.1 Research and Operations Partnership

AR Recon is a "Research and Operations Partnership" (RAOP) between multiple academic institutions, state and federal agencies, and stakeholders to improve forecasting of high-impact winter weather events in the Western U.S. (Ralph et al. 2020). The events relevant to AR Recon, in order of priority are:

- Strong landfalling AR along the U.S. West Coast
- Weak or moderate landfalling AR along the U.S. West Coast
- Cut-off low, with possible AR, to affect the Western U.S.
- Conditions over the northeast Pacific that may influence a major storm over the Central or Eastern U.S. (when there has been little AR activity along the U.S. West Coast)

Alongside gathering observations to improve NWP forecasts of significant weather events, AR Recon also acts to collect observations when the opportunity to improve scientific understanding is high. Sampling based on the latter motivation will produce results on a longer time scale than just considering improving an individual NWP forecast and can potentially lead to improvements in model skill by advancing both model and physical understanding.

3.2. AR Recon sequence

In AR Recon 2021 we defined an '*AR Recon sequence*' as a series of consecutive flights sampling the same synoptic system, with a maximum of one day gap between each set of flights. This targeted observation strategy was motivated by Zheng et al. (2021b) who identified positive impacts of AR Recon data on precipitation forecast skill that is maximized towards the end of each sequence flight, which they referred to as back-to-back IOPs every other day. Similar results were reported in Stone et al. (2020), which showed that the greatest observational impact on the forecast was in the last IOP during the first four IOPs in AR Recon 2018.

3.3. Essential atmospheric structures

The AR Recon 2021 sampling strategy focused on collecting targeted observations of synoptic-scale and mesoscale essential atmospheric structures within and proximal to ARs that are important for both forecast impact and scientific interest. Three tiers have been defined (Table 1), highlighting the relative importance of each feature for AR Recon targeting purposes.

The principal target was an AR itself (Tier 1), with sampling of mesoscale frontal waves (MFWs) the secondary Tier 1 target, as the small scale and rapid growth of them can modify the AR, presenting increased forecast challenges (Martin et al. 2019).

In Tier 2 are the synoptic-scale or sub-synoptic-scale disturbances within the jet stream, defined using winds at 250 hPa, which can create synoptic-scale ascent that aids the development of extra-tropical cyclones (e.g., Sanders and Gyakum 1980; Uccellini et al. 1985; Wash et al.1988; Wang and Rogers 2001; Yoshida and Asuma 2004) and are highly correlated with their spatial distribution on the seasonal scale (Zhang et al. 2017). Potential vorticity (PV) anomalies ('streamers') (Tier 2) are often linked to Rossby wave breaking (RWB) and are associated with intense stratosphere–troposphere exchange (e.g., Hoskins et al. 1985; Appenzeller et al. 1996; Sprenger and Wernli 2003) and have been shown to influence the evolution of surface weather (e.g., Hoskins et al. 1985), such heavy precipitation and flooding (Massacand et al. 1998; Martius et al. 2006, 2013; Ryoo et al. 2013). A warm conveyor belt (WCB) (Tier 2) is the airflow in an extratropical cyclone that ascends from the boundary layer to the upper troposphere along the vertically sloping isentropic surface (Carlson 1980), leading to cloud formation, precipitation, and latent heat release. In the lower troposphere, WCB parcels are apparent in the warm sector of extratropical cyclones and might be collocated with high values of IVT (i.e., AR conditions). Occurring with the WCB outflow region in the upper troposphere, close to the upper-level jet, are significant negative PV anomalies (Madonna et al. 2014a), which can generate upper-level anticyclonic circulation, and contribute to the formation of PV streamers downstream (Grams et al. 2011; Madonna et al 2014b).

An extratropical cyclone can intensify an AR via stronger wind, and the AR can enhance precipitation and release latent heat, contributing to the extratropical cyclone deepening (Zhang et al. 2019; Zhang and Ralph 2021). Therefore, gathering observations of this synoptic scale system is also a target of AR Recon (Tier 3). Narrow-cold frontal rainbands (NCFRs) (Tier 3) are 3–5 km wide, coinciding with the leading edge of an extratropical cyclone cold front, and associated with strong upward vertical velocities, intense rainfall (Hobbs 1978; Browning 1986; Jorgensen et al. 2003), and the potential for debris flows along the U.S. West Coast (e.g., Sukup et al. 2015; Oakley et al. 2017; Cannon et al. 2018, 2020).

	Feature	**Scale**	**References**
Tier 1	Atmospheric River (AR)	Synoptic	Ralph et al. 2017; Kamae et al. 2017
	Mesoscale frontal wave (MFW)	Mesoscale	Martin et al. 2019
Tier 2	Upper-level (250 hPa) jet*	Synoptic	Sanders and Gyakum 1980; Uccellini et al. 1985; Wash et al.1988; Wang and Rogers 2001; Yoshida and Asuma 2004; Zhang et al. 2017
	500 hPa PV streamer	Mesoscale	Massacand et al. 1998; Martius et al. 2006, 2013; Wernli and Sprenger 2007; Ryoo et al. 2013
	Warm conveyor belt (WCB)	Mesoscale	Carlson 1980; Wernli and Davies 1997; Grams et al. 2011; Madonna et al 2014a,b; Rodwell et al. 2018; Dacre et al. 2019

Tier 3	Extra-tropical cyclone	Synoptic	Zhang et al. 2019
	Narrow-cold frontal rainband (NCFR)	Mesoscale	Hobbs 1978; Hobbs and Persson 1982; Browning 1986; Jorgensen et al. 2003; Sukup et al. 2015; Oakley et al. 2017; Cannon et al. 2018, 2020

Although defined as distinct characteristics in Table 1, these essential atmospheric characteristics are inter-related and act on different scales, which poses modeling challenges. Several studies have highlighted the scale-dependence of atmospheric phenomena, e.g., Stull (1985), and Žagar et al. (2017), with predictability increasing with spatial scale and Lagrangian timescale.

*Table 1. Essential atmospheric structures listed in order of priority. *The upper-level jet can generally only be sampled by the NOAA G-IV, as the USAF C-130 flies too low. PV: Potential vorticity.*

These essential atmospheric features were analyzed in NWP forecasts of 1-5 days lead time and were used to plan flight tracks and dropsonde release locations. The principal forecasts used were the deterministic and ensemble versions of the NCEP GFS and the ECMWF IFS, with CW3E's high-resolution in-house Weather Research and Forecasting (WRF) Model (West-WRF), configured to optimally represent ARs and wintertime meteorology on the U.S. West Coast (Martin et al. 2018), available for additional analysis.

Forecasts of WCB activity were provided by colleagues at ETH Zürich, based on IFS forecasts (1° grid spacing, 137 model levels) (ECMWF, 2020). To identify WCBs, 48-h forward trajectories extending vertically from 1000 to 700 hPa (every 25 hPa) and horizontally separated by 80 km were analyzed using the Lagrangian Analysis Tool LAGRANTO (Wernli and Davies 1997; Sprenger and Wernli 2015). To be classified as a WCB trajectory, the 48-h ascent must exceed 600 hPa (Madonna et al. 2014a).

Several of these essential atmospheric structures were sampled during IOP 7, centered on 00 UTC 27th January including an AR, upper-level jet stream, and 500 hPa potential vorticity (PV) streamer (Figure 1a). These features were sampled by dropsondes, radiosondes and ARO, as well as drifting buoys, providing extensive coverage of the AR and surrounding area (Figure 1b). Although this system featured an NCFR, it was not sampled.

Figure 1. Sampling essential atmospheric structures and sensitivities in IOP 7, centered around 00 UTC 27th January 2021. a. Essential atmospheric structures present during IOP 7. NCEP GFS IVT at 00 UTC 27th January 2021: mean sea level pressure (MSLP) in black contour lines, IVT in orange filled contours, 500 hPa PVU in purple filled contours, precipitation in blue filled contour, 250 hPa jet in arrows. Dropsondes in black dots. NCFR: Narrow-cold frontal rainband.

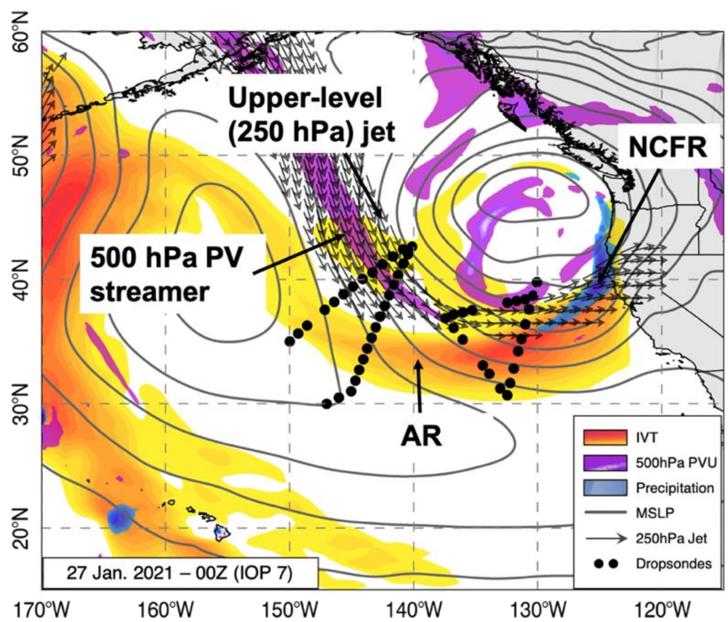

b) Observations taken during IOP 7, including dropsondes (black dots), radiosondes (green stars), buoy measurements (blue dots), ARO profiles (green lines). Flight tracks to and from Reno and Honolulu in black lines. NCEP GFS IVT at 00 UTC 27th January 2021: mean sea level pressure (MSLP) in black contour lines and IVT in orange filled contours.

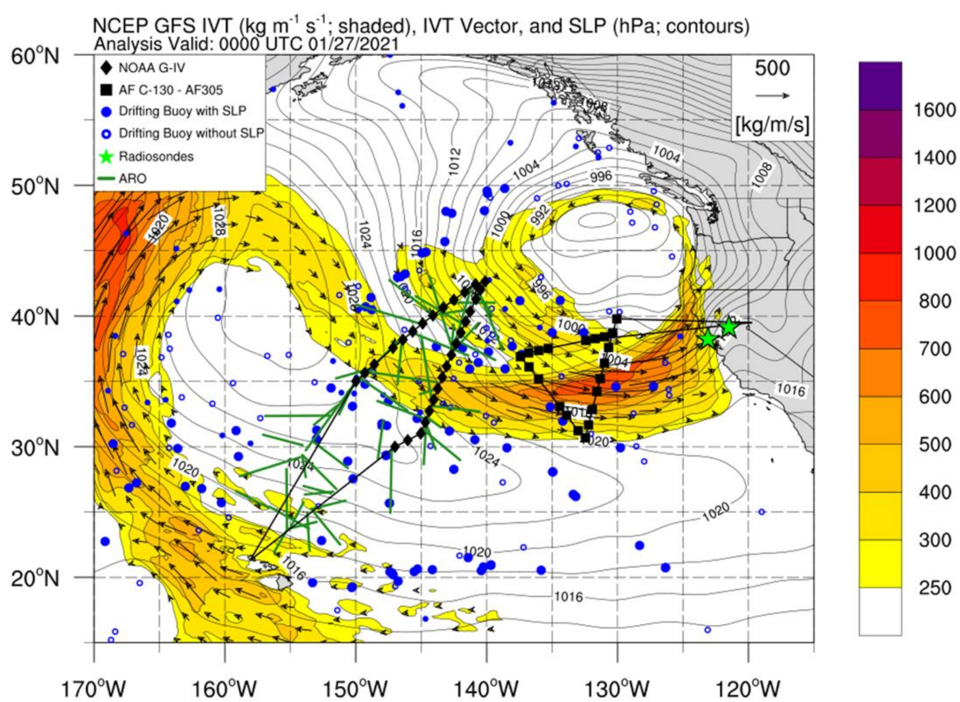

3.4 Sensitivity tools

Sensitive regions of the atmosphere indicate where uncertainty can grow quickly and often overlap with dynamically active areas. These regions are important to target with additional measurements, and the removal of observations in such sensitive areas has a larger negative impact on the forecast than removal of observations from random areas (Cardinali et al. 2007). AR forecasts may especially benefit from additional observations in sensitive regions because the areas in and around ARs have been identified as observation gaps, while quantitative tools also highlight these areas as particularly sensitive to initial condition errors (Doyle et al. 2019; Reynolds et al. 2019; Zheng et al. 2021a).

In AR Recon 2021, two different approaches to identify regions of forecast sensitivity were implemented: ensemble-based sensitivity that utilizes ECMWF, and a combination of NCEP Global Ensemble Forecast System (GEFS) and Canadian Meteorological Center (CMC) ensemble forecasts, and adjoint sensitivity using U.S. Naval Research Laboratory's (NRL's) Coupled Ocean–Atmosphere Mesoscale Prediction System (COAMPS) (Hodur 1997; Doyle et al. 2014; 2019), which has been utilized for targeted observing of tropical cyclones and ARs (e.g., Reynolds et al. 2010; 2019). Ensemble sensitivity tools analyze the linear relationships between a forecast metric and initial state variables to identify areas at the initial time or an earlier forecast time that are most sensitive to uncertainty growth at the verification time (Ancell and Hakim 2007; Torn and Hakim 2008; Torn and Hakim 2009; Chang et al. 2013; Zheng et al. 2013; Torn 2014; Hill et al. 2020). Adjoint models calculate forecast sensitivity of a response function to changes in the initial state (Errico 1997; Doyle et al. 2014; Rabier et al. 1996; Reynolds et al. 2019), where the largest values have the most impact on the forecast errors.

The most common response function was 24-hour accumulated precipitation over the U.S. West Coast, with approximately half of the IOPs focusing on precipitation over Northern California and Oregon, with two IOPs focused on sea level pressure over the Central Pacific/Northeast Pacific (Figure 2) and one IOP on precipitation in the Central U.S. The spatial distribution of response function domains in the GEFS and CMC ensemble sensitivity analysis (not shown) was largely the same as the ECMWF ensemble sensitivity (Figure 2a). Large domains were used to ensure that the sensitivity represented a change in magnitude and not a shift in location, signifying potential weakening or strengthening of the system with resultant precipitation changes.

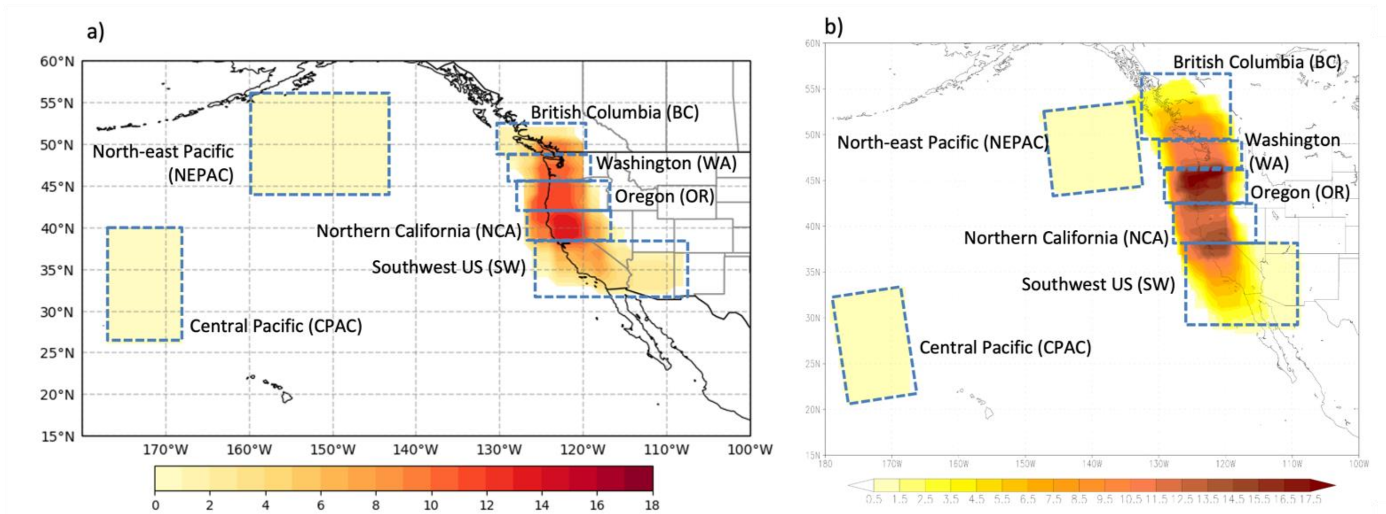

Figure 2. Heat map of response function domains for 28 IOPs (domain over central US, IOP 25, not shown) for a) ECMWF ensemble and b) COAMPS adjoint sensitivity. Units are number of IOPs. Note the GEFS and CMC contained similar distributions as panel (a) and are not shown.

Due to different response function domains and adjoint integration lengths, it is difficult to directly compare the magnitude of the sensitivities across each IOP. However, in AR Recon 2021, for the first time, the COAMPS adjoint sensitivity impact was calculated, defined as the optimal perturbation maximum magnitude for precipitation in the nonlinear model (measured in mm; Table S1). This value provides a comprehensive metric to understand the potential for error growth, which was categorized into low (0-5), medium (5-10), and high (10+) mm.

The COAMPS sensitivities for IOP 7 (Figure 3) highlight the sensitivity of the precipitation forecast to changes in the initial potential temperatures, specific humidity, potential vorticity (PV), and winds within the upstream region of high IVT but also within the low pressure itself. These general sensitivity characteristics are typical for both North Atlantic and northeastern Pacific cyclones and ARs (Doyle et al. 2014, 2019; Reynolds et al. 2019). The COAMPS adjoint sensitivity impact for IOP 7 was almost 22 mm, which is considered high in this analysis (see Table S1).

The ECMWF ensemble sensitivities (Figure 4) show that the strongest IVT and equivalent potential temperature (θ_e) sensitivities are concentrated in the IVT plume, and the 500 hPa PV streamer aligned with the upper-level jet, similar to the COAMPS result (Figure 3). The GEFS and CMC ensemble sensitivity (not shown) showed largely similar spatial patterns as the ECMWF ensemble sensitivity. The summaries (Figures 3d, 4d) show the vertically integrated sensitivities for both analyses, highlighting dropsonde sampling of the AR itself, along with sampling wide areas of relatively large sensitivity, which is preferable to targeting a specific high sensitivity value. Note that this assessment highlights the sensitivity fields of select variables, but many others can be used, for example atmospheric refractivity, which can help to inform decisions on flight paths that can optimize ARO measurements within the constraints of the desired dropsonde pattern.

Figure 3. COAMPS adjoint sensitivity of 24-h accumulated precipitation (12 00 UTC 27 Jan - 12 00 UTC 28 Jan), initialized 00 UTC 25 Jan, for IOP 7: 00 UTC 27 Jan. Locations of dropsondes marked as circles. Response function domain marked as a green box. a) 850-hPa potential temperature sensitivity (color fill; colorbar every 10^{-3} mm $(°C)^{-1}$) and 850-hPa potential temperature (isotherms every 2.5°C), b) 500-hPa PV adjoint perturbation (color fill; colorbar every 0.01 PVU) and 500-hPa PV (contours every 0.1 PVU,) c) 850 hPa water vapor sensitivity (color fill; colorbar every 20^{-3} mm $(g\ kg^{-1})^{-1}$) and 850-hPa specific humidity (contours every 1 g kg^{-1}), d) Summary figure with vertically integrated water vapor sensitivity (blue contours and color fill; colorbar every 10 mm $(g\ kg^{-1})^{-1}$), vertically integrated wind sensitivity (red contours every 2 mm $(m\ s^{-1})^{-1}$), IVT forecast field (gray contours every 250 kg m^{-1} s^{-1}), and PV optimal perturbations (green stippling 20-40 PVUs and purple stippling 40 PVUs and above). The sensitivities are scaled by 10^5 $km^3/(\Delta x \Delta y \Delta z)$.

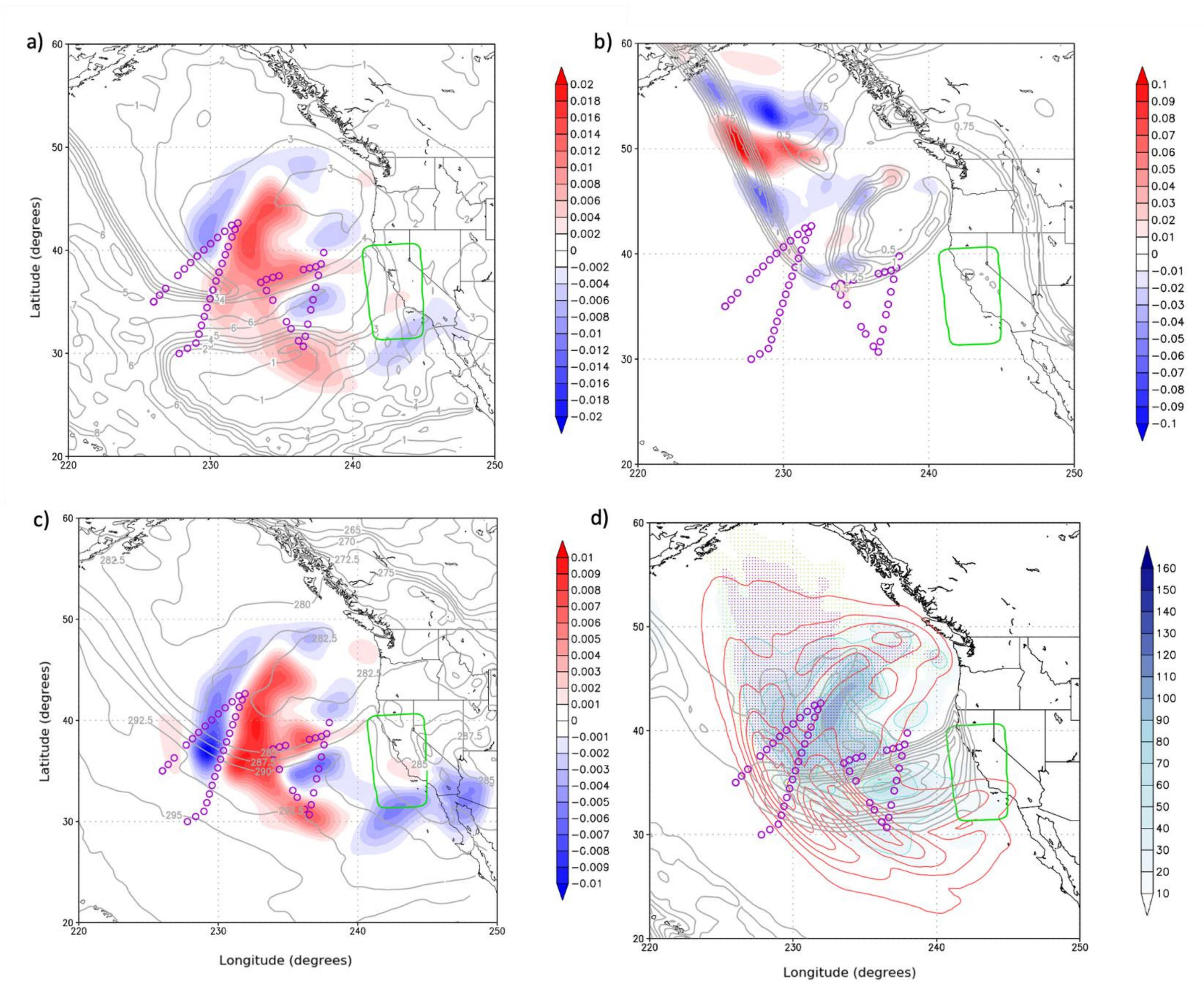

Figure 4. ECMWF ensemble sensitivity of 24-h accumulated precipitation (12 00 UTC 27 Jan - 12 00 UTC 28 Jan), initialized 00 UTC 25 Jan, for IOP 7: 00 UTC 27 Jan. Locations of dropsondes marked as circles. Response function domain marked as a green box. a) 850 hPa equivalent potential temperature (θ_e) sensitivity (colored contours) and 850 hPa θ_e ensemble mean (contour lines). b) 500 hPa PV sensitivity (colored contours) and 500 hPa PV ensemble mean (contour lines). c) IVT sensitivity (colored contours) and IVT ensemble mean (contour lines). d) Summary figure with IVT sensitivity (blue contours from 0.3 magnitude, every 0.1) vertically integrated θ_e sensitivity (cyan contours from 0.2 magnitude, every 0.1) vertically integrated PV sensitivity (purple stippling from 0.3 magnitude) IVT forecast field (yellow filled contours, 250 kg m^{-1} s^{-1} and above). The sensitivity fields are dimensionless as the metric is the principal component of the precipitation EOF pattern.

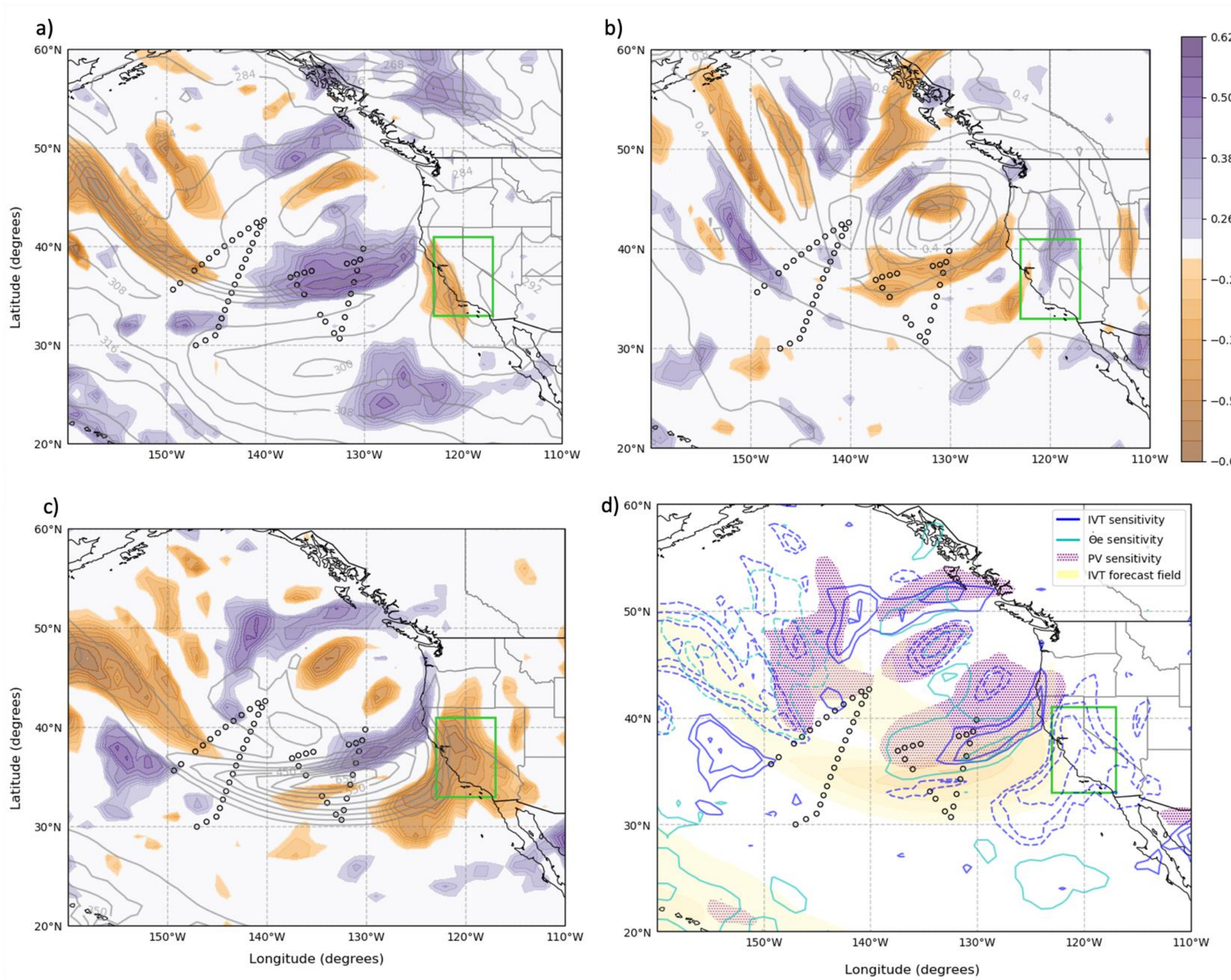

.

3.5. Operational considerations

During AR Recon 2021, the NOAA G-IV was based in Hawaii, and the USAF was based in Reno with two C-130s, relocating to Sacramento for the final week of the season (17th March). All aircraft were available for a first possible flight centered at 00 UTC 15th January, with the last possible flight for the G-IV on 00 UTC 14th March, whereas the USAF C-130s were available until the end of March. Depending on aircraft and crew availability, it was possible to deploy up to three aircraft in a single IOP. The dropsonde window of focus was 2030-0230 UTC (1230-1830 PST), providing data for the 6-h assimilation time window centered at 00 UTC. In general, the C130s and G-IV deployed 25 and 30 dropsondes, respectively, with approximately 130-150 km spacing. However, there were select IOPs during which a higher rate of deployment was requested (~110 km spacing) in the vicinity of mesoscale features, for example PV streamers, and this maximum rate was limited by the time taken to deploy. In some cases, during which not all targets could be reached within the drop window, dropsondes were deployed outside of the 00 UTC assimilation window. It was preferable to gather these extra dropsonde observations within the 18Z assimilation window rather than 06Z assimilation window, as this should improve the accuracy of the 18Z forecast that provides the first guess, or background state, for the 00 UTC cycle. All flight tracks were limited to approximately 3200 nautical miles (nm) and restricted air space was considered. Although discussion about potential targets began up to 4 days prior, all flight tracks and dropsonde release locations were finalized at approximately 1800 UTC on the day prior to takeoff, 30 hours before 00 UTC IOP centered time.

4. Observational data collected during AR Recon 2021

During AR Recon 2021 there were 29 successful IOPs, 27 C130 flights, 18 G-IV flights, six sequences and 1142 viable dropsondes; an increase of 12 IOPs and 404 dropsondes compared to 2020. Table S1 provides details including the forecast impact and research questions, sensitivity analysis, and observations collected. Moderate and weak ARs were sampled, as well as a cutoff low (Figure 5a) that was forecast to eventually move onshore and lead to large downstream development to the lee of the Rockies (see Section 1.1). The largest accumulated precipitation amounts (more than 700 mm during AR Recon 2021) were in Northern California, Oregon, and Washington, in regions where the sampled AR tracks made landfall. The NOAA G-IV released ten dropsondes along its returning flight track from Honolulu to Long Beach, CA (00 UTC 16th March). This was not a true IOP as the flight track was not planned according to the sampling strategy, and so was designated IOP 28.5.

In AR Recon 2021, 23 out of 29 IOPs were part of a sequence, (Table 2) which comprised a set of IOPs that sampled the same synoptic system over multiple days (Section 3.2). All sequences in AR Recon 2021 consisted of IOPs on consecutive days, although a one-day gap between each IOP is acceptable.

Table 2. AR Recon 2021 sequences. IOP 25 is split into two sequences, with the C-130 flight in sequence 5, and the G-IV flight in sequence 6.

Sequence	Number of IOPs (IOP numbers)	Dates	Number of G-IV flights	Number of C-130 flights	Total number of dropsondes
1	6 (IOP 3-8)	23, 24, 25, 26, 27, 28 January	6	4	261
2	3 (IOP 9-11)	31 January, 1, 2 February	2	3	125
3	3 (IOP 16-18)	23, 24, 25 February	2	1	80
4	3 (IOP 19-21)	3, 4, 5 March	-	3	70
5	4 (IOP 22-25)	8, 9, 10, 11 March	2	4	162
6	4 (IOP 25-28)	11, 12, 13, 14 March	4	3	177

Figure 5. AR Recon observations

a) Summary of IOPs sampled during AR Recon 2021, with arrows indicating where the orientation and location of the AR when it was strongest over the coast during the IOPs. Stage IV precipitation during AR Recon 2021. Grey dashed line indicates a low pressure system that was targeted.

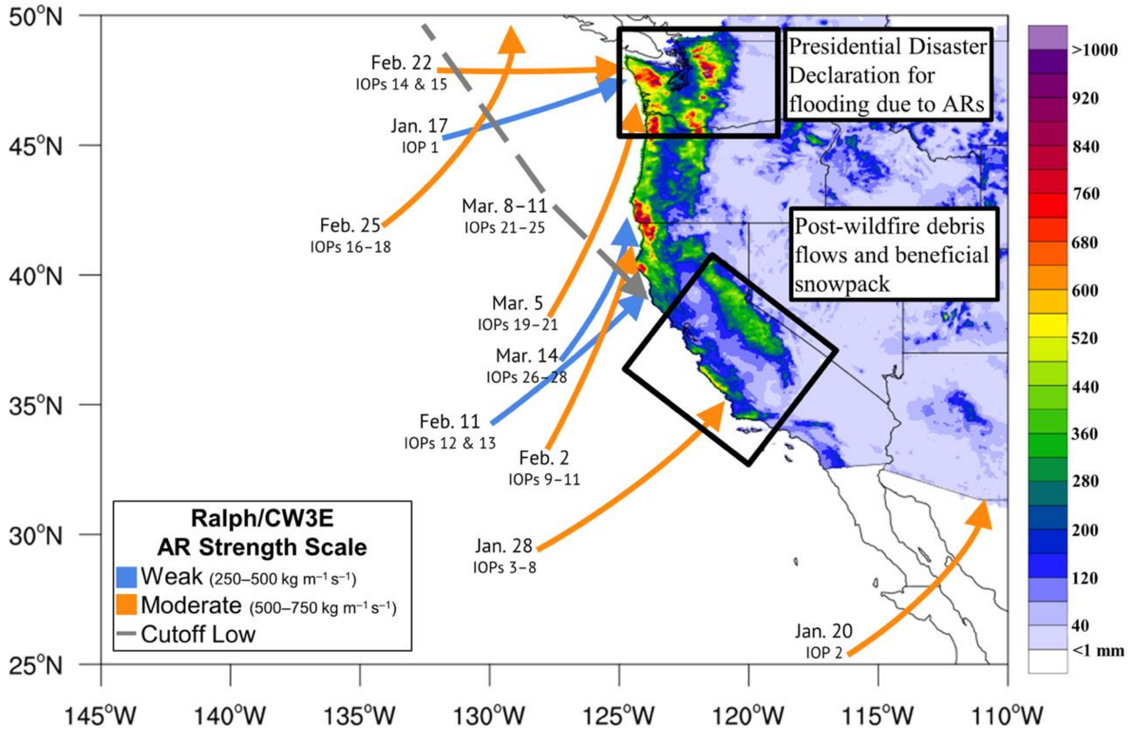

b) Timeline with cumulative count of successful dropsondes deployed during AR Recon 2021. IOP number and sequences labelled. Total number of successful dropsondes: 1142.

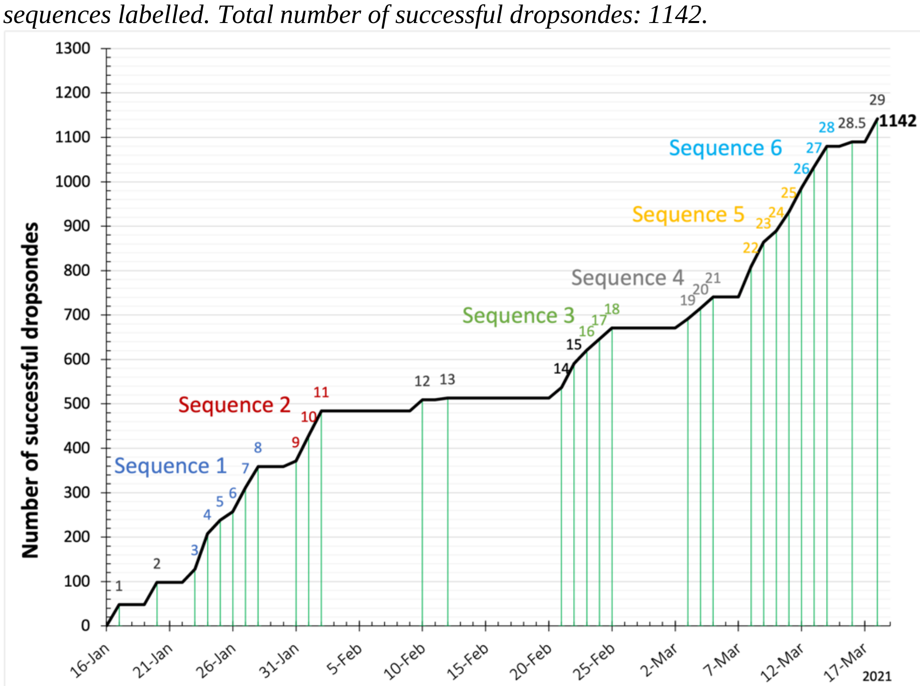

c) AR Recon 2021 dropsonde release locations, color-coded by sequence. 1500 nm radii from Honolulu and Reno shown in black dashed arcs. Grey contour shading AR days from Rutz et al. (2013). Domains based on WMO ocean sectors shown in dashed blue boxes.

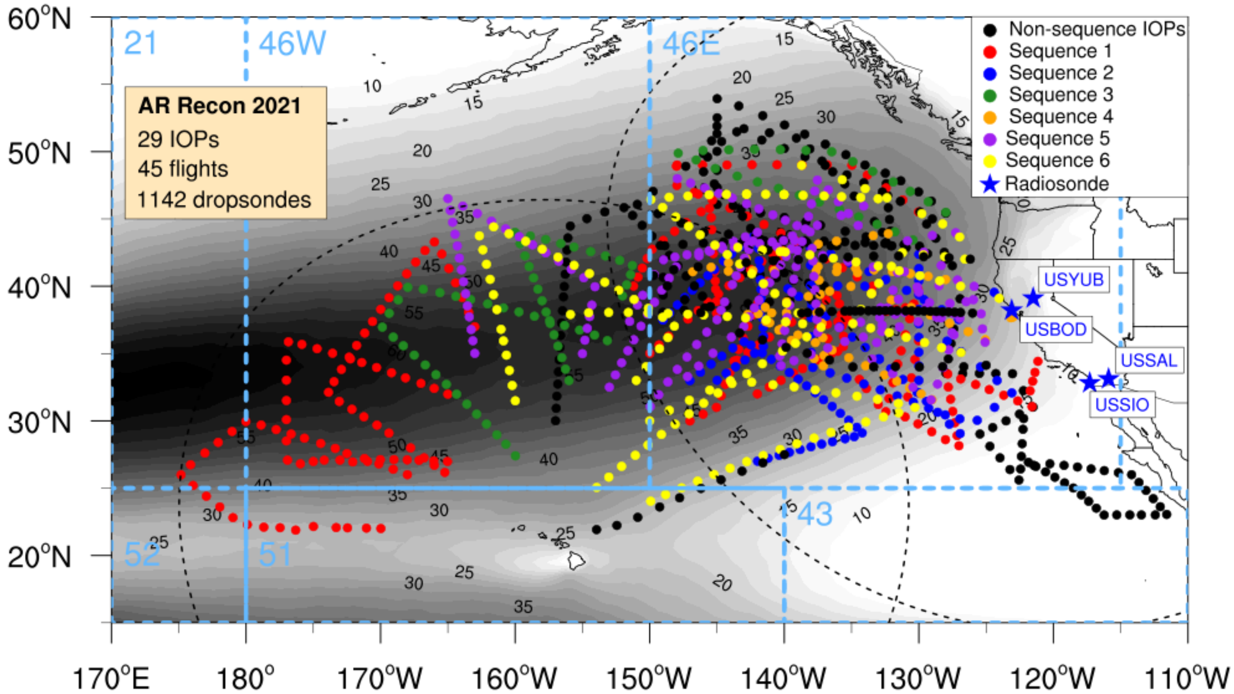

d) Probability density of dropsonde IVT sampled during AR Recon 2021, all dropsondes (blue), dropsondes with IVT >=250 (kg m^{-1} s^{-1}) (orange). e) Probability density of dropsonde IVT by sector. Non-AR cold side (NCS), AR cold sector (CS), AR core (C), AR warm sector (WS), non-AR warm side (NWS).

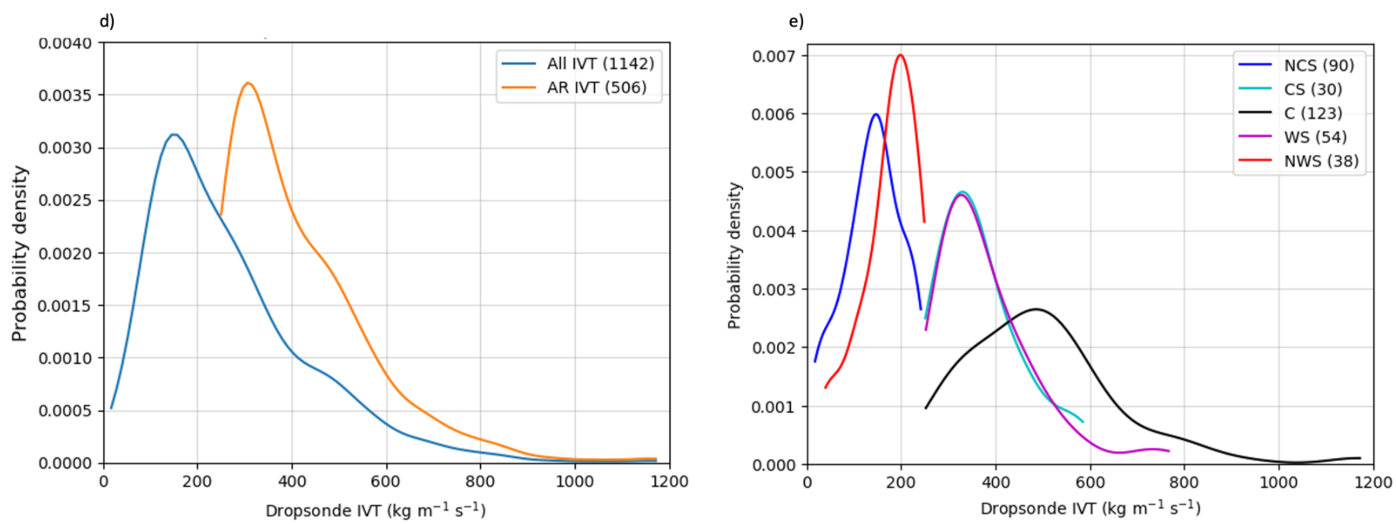

4.1 Dropsondes

There were 1142 successful dropsondes deployed (Figure 5b), with an additional 110 that failed (~9%). When failure occurred, repeat dropsondes were used, resulting in a total of 1252 dropsondes deployed. These dropsondes spanned 22°N - 55°N and 175°E - 112°W, with the highest density in the 46E domain (based on WMO ocean sectors, Figure 5c). This domain is within reach of the two C-130s and represents sampling closer to landfall, with 46W mostly only within reach of the single G-IV based in Hawaii and is further upstream, permitting sampling at a longer lead time. The USAF C130s released dropsondes at an altitude of ~8 km (~350 hPa), compared to the NOAA G-IV at an altitude of ~12 km (~200 hPa) (Cobb et al. 2021b, Figure S1), with only the latter aircraft able to fully sample the upper-level jet.

The frequency maximum of the dropsonde IVT distribution is just below 200 kg m^{-1} s^{-1}, with the tail of the distribution reaching a maximum value of 1150 kg m^{-1} s^{-1} (blue line in Figure 5d). Considering just dropsondes with IVT greater than the 250 kg m^{-1} s^{-1} threshold (widely considered the minimum threshold for an AR, e.g., American Meteorological Society 2019), the peak of the distribution is 300 kg m^{-1} s^{-1}, which represents weak AR strength according to Ralph et al. (2019). Three weak and six moderate ARs were sampled in 2021 (Figure 5a), and this low-IVT shifted distribution of dropsonde IVT also highlights the relatively dry conditions that have led to persistent drought (Section 2).

Dropsondes can also be separated into which AR sector they are sampling, using the method detailed in Cobb et al. (2021a), in which the following sectors were identified: Non-AR cold side (NCS), AR cold sector (CS), AR core (C), AR warm sector (WS), non-AR warm side (NWS). We identified 36 AR transects over 22 IOPs, in which the line of dropsondes was deployed approximately perpendicular to the AR axis. The non-AR cold and warm sides have values less than the AR threshold, and the core is the highest IVT region, with a peak distribution at ~500 kg m^{-1} s^{-1} (Figure 5e). The IVT distribution of the AR cold and warm sectors is almost identical, in line with results from Cobb et al. (2021a). The remaining dropsondes that did not form AR transects (807 of 1142) comprised of partial AR sampling that was not sufficient to determine sectors across a full transect, as well as sampling of other non-AR targets (Section 1.2.2, Table 1), or areas highlighted in the sensitivity analysis (Section 1.2.3).

4.2 Airborne Radio Occultation (ARO)

Airborne Radio Occultation (ARO; Haase et al. 2014) uses Global Navigation Satellite System (GNSS) signal delays to retrieve refractivity profiles to the sides of the aircraft that can penetrate thick clouds and precipitation. Atmospheric refractivity is a sensitive indicator of vertical moisture structure and tropopause structure in the frontal region. The system is operating in research mode on the NOAA G-IV, collecting data to evaluate the potential for the observations to improve model initial conditions (Haase et al. 2021, submitted), and is also being evaluated for flights on the USAF C-130s. In the first 6-flight sequence (IOPs 3-8), 271 profiles were collected (roughly 5.8 per hour) with 224 inside the 6-hour window centered at 00 UTC. Figure 6a shows the lowest ARO tangent points for each occultation collected during AR Recon 2021, totaling 804 (Table S1), and highlights the large area that was sampled, complementing the dropsondes released from the aircraft (Figure 5c).

4.4 Drifting Buoys

A total of 30 drifting buoys with barometers were deployed in regions 51, 46W and 46E in partnership with the USAF during January 2021 before the start of flight planning (Figure 6b). Ten of these buoys were Directional Wave Spectra-Barometer (DWS-B) buoys and twenty were Surface Velocity Program - Barometer (SVP-B) buoys. Fewer buoys were deployed than in 2020, when 64 total drifting buoys were deployed, due to challenges from the global pandemic (Section 6). Buoys report data every 15 minutes and generally last for 1-1.5 years in the case of SVP-B and 6-8 months in the case of DWS-B.

Buoy deployment targeted areas that did not have existing drifting buoys with pressure sensors and that were within climatologically active storm tracks (Figure 6b). The buoys vary greatly in drift distance; the 2021 buoys drifted an average of 498 km (range 57-975 km) from deployment, over the following three months (Figure 6c). These 30 drifting buoys supplemented 50 drifting buoys from prior years that were still reporting, and 53 drifting buoys with pressure that were deployed outside of AR Recon. AR Recon enabled ~60% of drifting buoys within the domain to observe pressure; without AR Recon this number would have been 38%. Evaluation is ongoing to determine the impact of these extra observations on forecasts during AR Recon (Subramanian et al. 2021).

4.5 Radiosondes

During select AR Recon flights, specifically those which targeted precipitation in California or farther inland, radiosondes were released at up to four locations in California simultaneously: Yuba (YUB), Bodega Bay (BOD), Scripps Institution of Oceanography (SIO), and Salton Sea (SAL) (Figure 6d, Table S1). Each radiosonde records pressure, temperature, and relative humidity four times per second, with wind and height also reported via GPS. Radiosondes generally reach ~20 km in altitude before descent, although the signal can be lost much earlier. Radiosondes released during this campaign were equipped with parachutes and continued to record and transmit data during descent. Three radiosondes per location were released during flight times, every three hours, and more were released if there were AR conditions (IVT > 250 kg m^{-1} s^{-1}) at the launch site, resulting in a total of 111 released as part of AR Recon 2021. The deployment of these radiosondes was funded by Forecast Informed Reservoir Operations (FIRO) campaigns in Lake Mendocino (Jasperse et al. 2020) and Prado Dam (Ralph et al. 2021).

All AR Recon dropsonde, radiosonde, and buoy data were distributed in real time, when possible, via the GTS for operational NWP assimilation. The ARO data as well as the NOAA G-IV tail Doppler radar (TDR), which recorded data in areas of forecast precipitation, were not available in real time, but are extremely useful for process-based studies after the event (e.g., Norris et al. 2020).

Figure 6. AR Recon ARO, drifting buoy, and radiosonde observations

a) Location of the lowest ARO tangent points for each occultation collected during AR Recon 2021.Circles indicate profiles inside the 6-hour window at 00 UTC, with filled symbols indicating profiles that extended from flight level down below 3 km, open symbols indicate profiles that terminated above 3 km. x indicates profiles during flight that were recoded outside the 6-hour window.

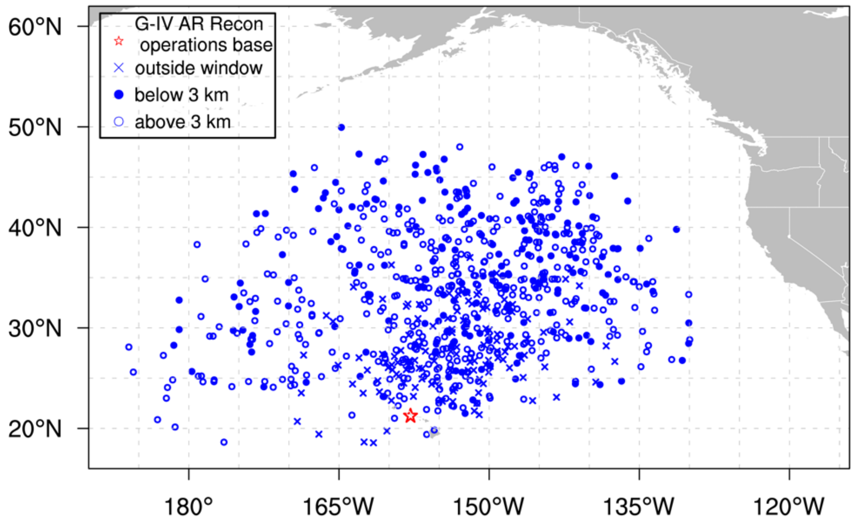

b) Drifting buoy locations in the northeast Pacific, with those released during AR Recon 2021 shown in green. GDP: Global Drifter Program. SLP: sea level pressure. SVP-B: Surface Velocity Program – Barometer. DWS – B: Directional Wave Spectra Barometer. Grey contour shading AR days from Rutz et al. (2013).

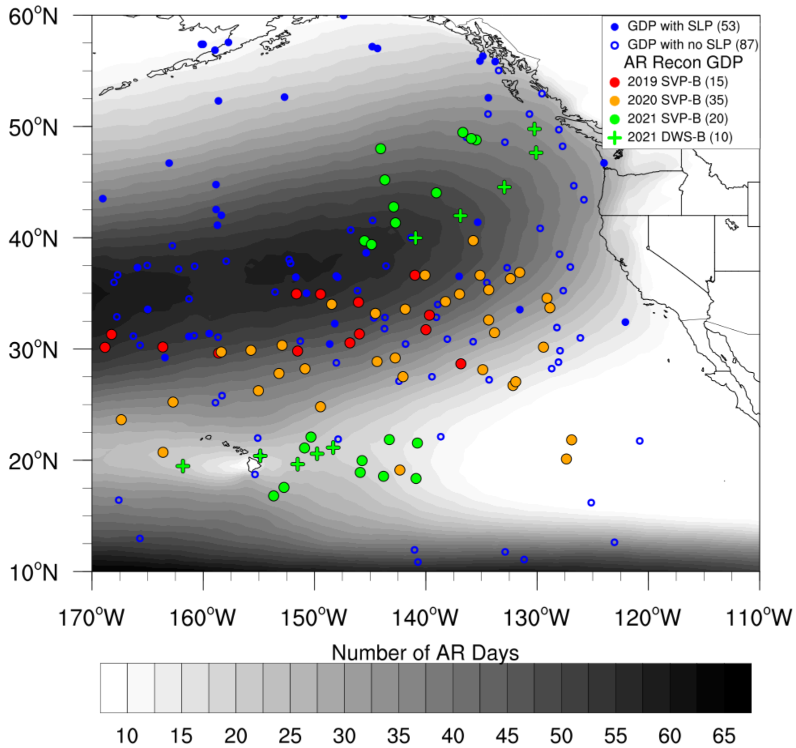

c) Change in location of AR Recon drifting buoys during the AR Recon 2021 season (red, orange, blue). Black outlined dots represent starting position of buoy, non-outlined dots represent ending position.

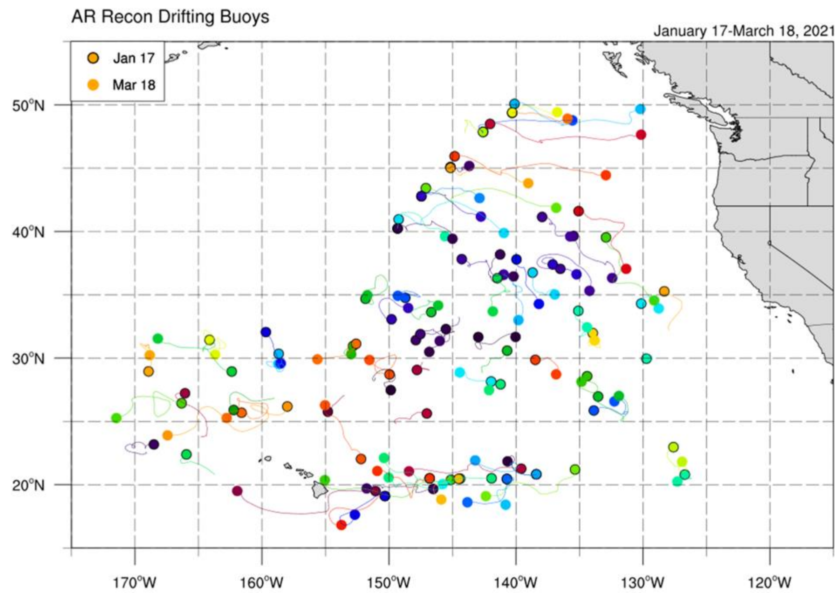

d) Radiosonde soundings during AR Recon 2021. Map showing the launch locations and chart showing dates/number released. Terrain background. USYUB: U.S. Yuba; USBOD: U.S. Bodega Bay; USSIO: Scripps Institution of Oceanography; USSAL: Salton Sea.

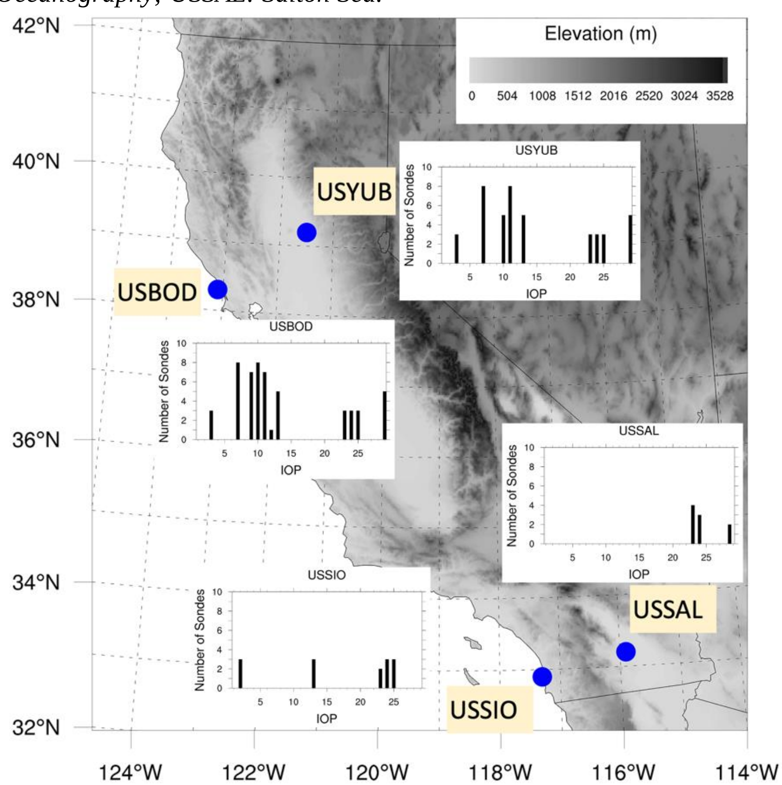

5. AR Recon 2021 assimilated data

Alongside models from the operational centers directly involved with AR Recon (NCEP GFS, ECMWF IFS and NRL NAVGEM and COAMPS), several other models also assimilated AR Recon 2021 data (Table 3). Additional centers that gathered observational data from the GTS also had access to AR Recon 2021 data, although not all are detailed here.

Table 3. NWP models that assimilated AR Recon 2021 data.

Center and model	**Country**
National Aeronautics and Space Administration (NASA) Global Modeling and Assimilation Office (GMAO) Goddard Earth Observing System (GEOS)	USA
UK Met Office Unified Model (MetUM)	UK
Environment Canada Global Environmental Multiscale Model	Canada
Japan Meteorological Agency (JMA) Global Spectral Model (GSM)	Japan
Météo- France Action de Recherche Petite Echelle Grande Echelle model (ARPEGE)	France
Australian Community Climate and Earth-System Simulator (ACCESS-G)	Australia

Figure 7 shows the number of dropsondes assimilated in real-time into GFS, NAVGEM and IFS operational forecast models in the 18, 00, and 06 UTC (GFS and NAVGEM), and 12 and 00 UTC (ECMWF) assimilation windows. The vast majority of dropsonde data was assimilated in the 00 UTC window, around which the targeted observations were centered. There is considerable variability in the number of dropsondes released during each IOP due to the number of aircraft used and mechanical issues, with a maximum of 80 in IOP 4 and only four successful dropsondes released during IOP 13. In 25 out of 29 IOPs, 100% of dropsondes were assimilated in real-time into GFS and NAVGEM operational forecast models (Figure 7). However, 100% of dropsondes were assimilated by ECMWF in only 4 IOPS, with considerably fewer in several cases, likely due to issues with the data transmission or thinning in the ECMWF NWP system.

Dropsonde observations taken by the C130 during the 00 UTC January 24 (IOP 4) update cycle were not assimilated in real time by ECMWF or NOAA due to an issue with the connection between the USAF 557th Weather Wing and National Weather Service (NWS). However, they were received and assimilated by the Navy models through the (typically redundant) Department of Defense (DoD) automated weather network.

The total number of AR Recon 2021 wind, temperature, and moisture dropsonde data points assimilated into the GFS operational model is shown on the levels that each variable was assimilated, as well as the sum across several levels, for inter-comparison (Figures 8a,b,c). From 800 to 600 hPa and 600 to 400 hPa, more than double the number of temperature and moisture data points (6000-7000) are assimilated compared to wind (2000-3000). However, in the lowest level (1200 – 1000 hPa), the number of wind observations is almost double that of temperature and moisture, which are nearly identical. Specific humidity (Figure 8c) is only assimilated up to 300 hPa because it is too dry above this threshold, whereas temperature and winds are assimilated up to 50 hPa (Figures 8a,b). From 300 to 50 hPa, there are more than 50 % more wind data points assimilated than temperature. These findings motivate further research into the exploration of the data assimilation systems to examine why certain data are excluded. However, this is beyond the scope of this paper.

Although the dropsondes record very high vertical resolution data, only the full profile (i.e., Binary Universal Form for the Representation of meteorological data (BUFR)) data from dropsondes deployed by the NOAA aircraft were available in real-time to the GTS and for assimilation into operational NWP. The USAF data were transmitted to the GTS in Traditional Alphanumeric Code (TAC) format, which has significantly reduced vertical levels (i.e., mandatory and significant levels). The GFS model that was operational during AR Recon 2021 was unable to assimilate BUFR data, so all dropsonde data was assimilated on much reduced levels. Unlike the assimilation of BUFR data, TAC data is only assimilated at the release location's horizontal coordinates, with no account for dropsonde drift.

Alongside the targeted observations collected as part of AR Recon, there are a vast array of other observations collected over the northeast Pacific as part of the conventional observing system. Examination of data assimilated in the operational GFS model valid for analysis at 00 UTC January 27 (IOP 7) shows that GPS RO coverage is relatively well spread across the domain (at least to 40^0N) and does not seem to be affected by the presence of the AR at any level (Figures 9b,d,f). The aircraft data are only gathered in the upper troposphere and are not affected by the presence of the AR (Figure 9b), which is focused in the lower troposphere. In the middle troposphere, there are scarce atmospheric motion vector (AMV) data, and this makes it difficult to examine whether the presence of AR conditions has any effect. In the lower troposphere, there are widespread AMV data, and a data void is apparent in the core of the AR (Figure 9e), consistent with Zheng et al. (2021a). Marine surface observations are significantly increased because of the AR Recon drifting buoys deployed annually beginning in 2019 (Lavers et al. 2020c). Consistent with Zheng et al. (2021b), most assimilated radiance data in GFS are clear sky radiance data, which are limited within ARs, and although all sky radiances are assimilated in cloudy areas, they are typically assigned smaller weights than clear sky data (Zhu et al. 2016). There is an increase in lower troposphere wind observations and GPS RO data at all levels compared to results in Zheng et al. (2021a), mainly due to the availability of atmospheric motion vector products from the Geostationary Operational Environmental Satellite (GOES) – R Series (e.g., Schmit et al. 2017), and the newly launched COSMIC-II (Schreiner et al. 2020; Ruston and Healy 2020). This highlights the value of the AR Recon dropsondes, which can collect data at high vertical resolution throughout the depth of the atmosphere, where conventional observing systems may be lacking.

Several previous studies have shown the positive impact of these data on AR forecasts (e.g., Stone et al. 2020; Tallapragada et al. 2021; Zheng et al. 2021b), and data denial experiments that systematically assess data impact of the AR Recon 2021 targeted observations are beyond the scope of this paper but are underway. We can, however, illustrate the impact of all observations on the analysis in the ECMWF IFS. Figure 10 shows the observation-minus-background (O-B) and observation-minus-analysis (O-A) departures for the wind speed, temperature, and specific humidity in the BUFR and TAC dropsondes. Following the data assimilation procedure, the analysis draws closer to the dropsonde observations, and there is a suggestion of a cold bias in the background temperature forecasts (Figures 10b,e), a result that corroborates the findings in Lavers et al. (2020a). For the specific humidity, there is evidence that the O-B and O-A departures have larger spread near 850 hPa above the planetary boundary layer (Figures 10c,f) which may signify a model issue with positioning the moisture correctly with height or an issue representing the correct height of the boundary layer. Zheng et al. (2021a) found that the RMS fit for humidity using dropsondes and the GFS model analysis is also largest between 600-850 hPa and Stone et al. (2020) also find a maximum in temperature O-B standard deviations near 850 hPa. These large discrepancies between dropsonde observations and the forecasts in both models likely signify a model issue with positioning the moisture correctly with height.

Figure 7. AR Recon dropsonde data assimilated in GFS, NAVGEM and ECMWF.

Total number of dropsondes released in each IOP (blue bars). Number of dropsondes assimilated during each IOP into GFS (filled orange circle) (18Z +00 UTC + 06Z), NAVGEM (blue circle) (18Z +00 UTC + 06Z), and ECMWF (green cross) (12Z +00 UTC). Number of dropsondes assimilated in GFS and NAVGEM (18Z + 06Z) and ECMWF (12Z) as small markers.

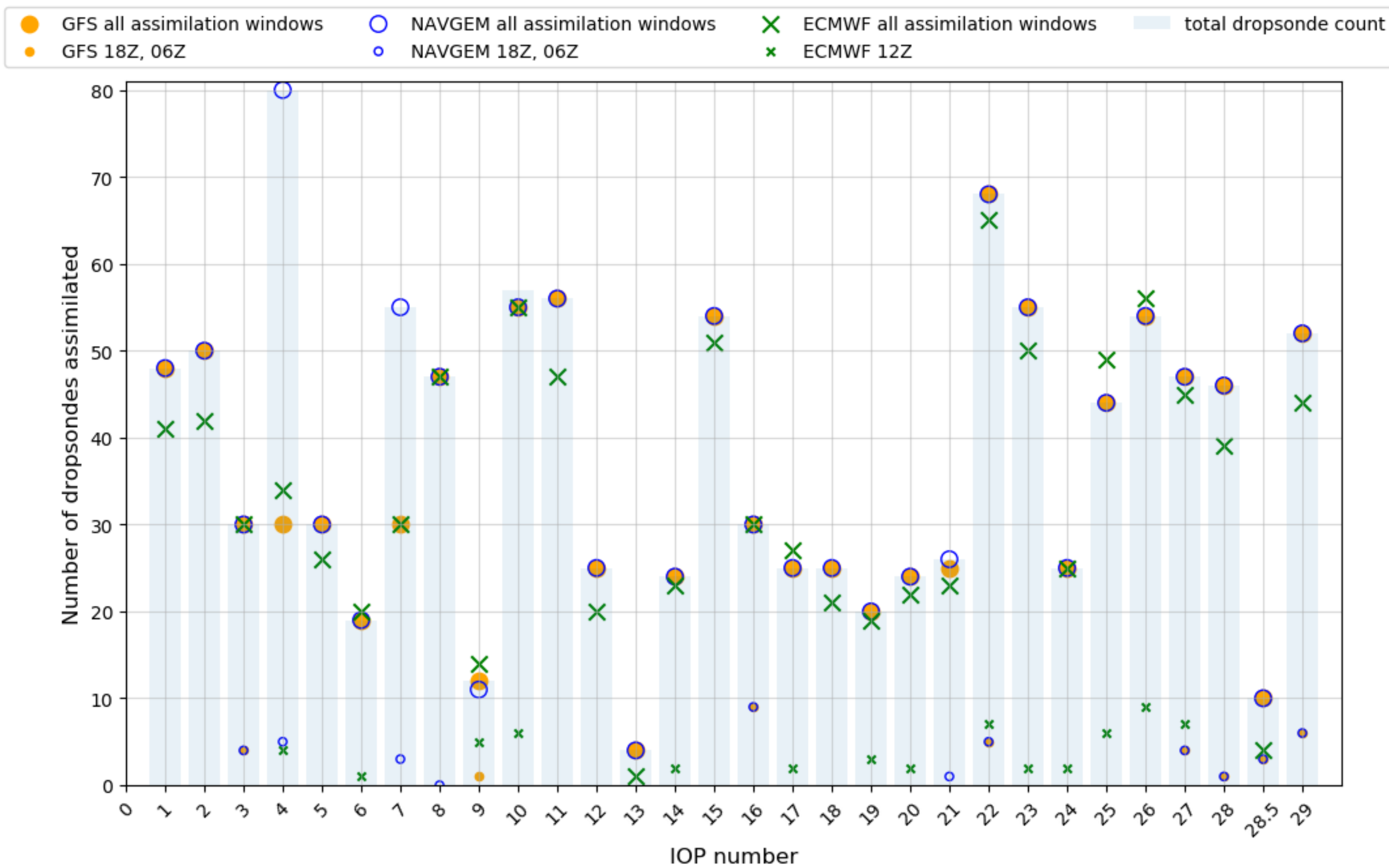

Figure 8. Total number of dropsonde data points assimilated into GFS during AR Recon 2021. a) Wind assimilated in 11 levels (1200-1000, 1000-900, 900-800, 800-600, 600-400, 400-300, 300-250, 250-200, 200-150, 150-100, 100-50 hPa. b) Same as (a) but for temperature. c) specific humidity assimilated in 10 levels (1200-1000, 1000-950, 950-900, 900-850, 850-800, 800-700, 700-600, 600-500, 500-400, 400-300 hPa). Secondary y axis is sum of pressure levels, consistent across all variables, for comparison.

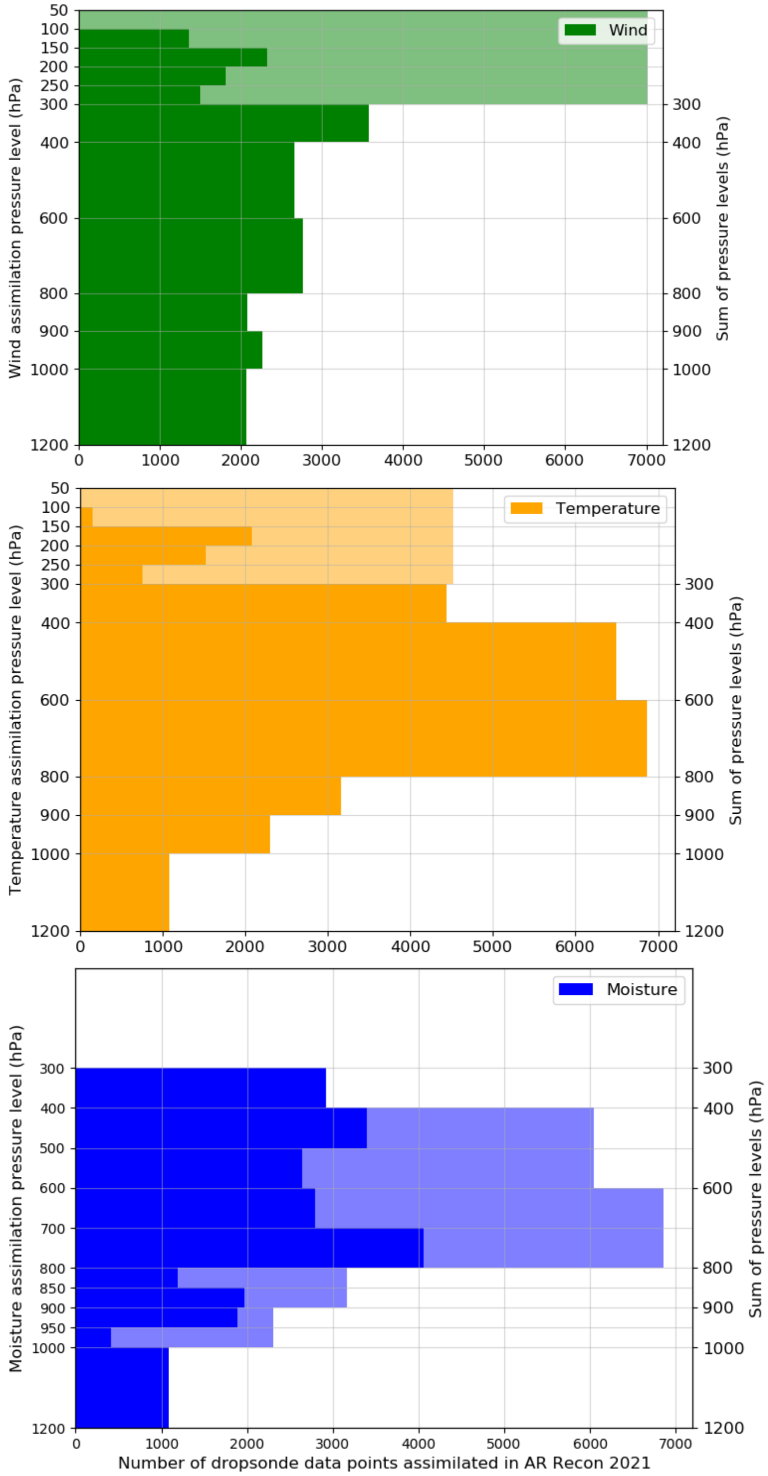

Figure 9. Data assimilated in the operational GFS model valid for analysis at 00 UTC January 27, 2021 (IOP7) from the conventional observing system. a),b) upper-troposphere (200–449 hPa); c),d) middle-troposphere (450–699 hPa), and e), f) lower-troposphere (pressure ≥ 700 hPa) and the surface. Panels on the left are for the wind observations, including direct wind data, atmospheric motion vector (AMV), and the velocity azimuth display wind (VADWND), and on the right are for the rest variables, including temperature, humidity, surface pressure, sea surface temperature, and GPS radio occultation (GPSRO). IVT (kg m^{-1} s^{-1}) in the operational GFS analysis in yellow filled contours. Non-radiance data include conventional and non-radiance remote sensing data. Note "AR Recon Dropsondes" represents the dropsondes collected during AR Recon 2021 IOP7.

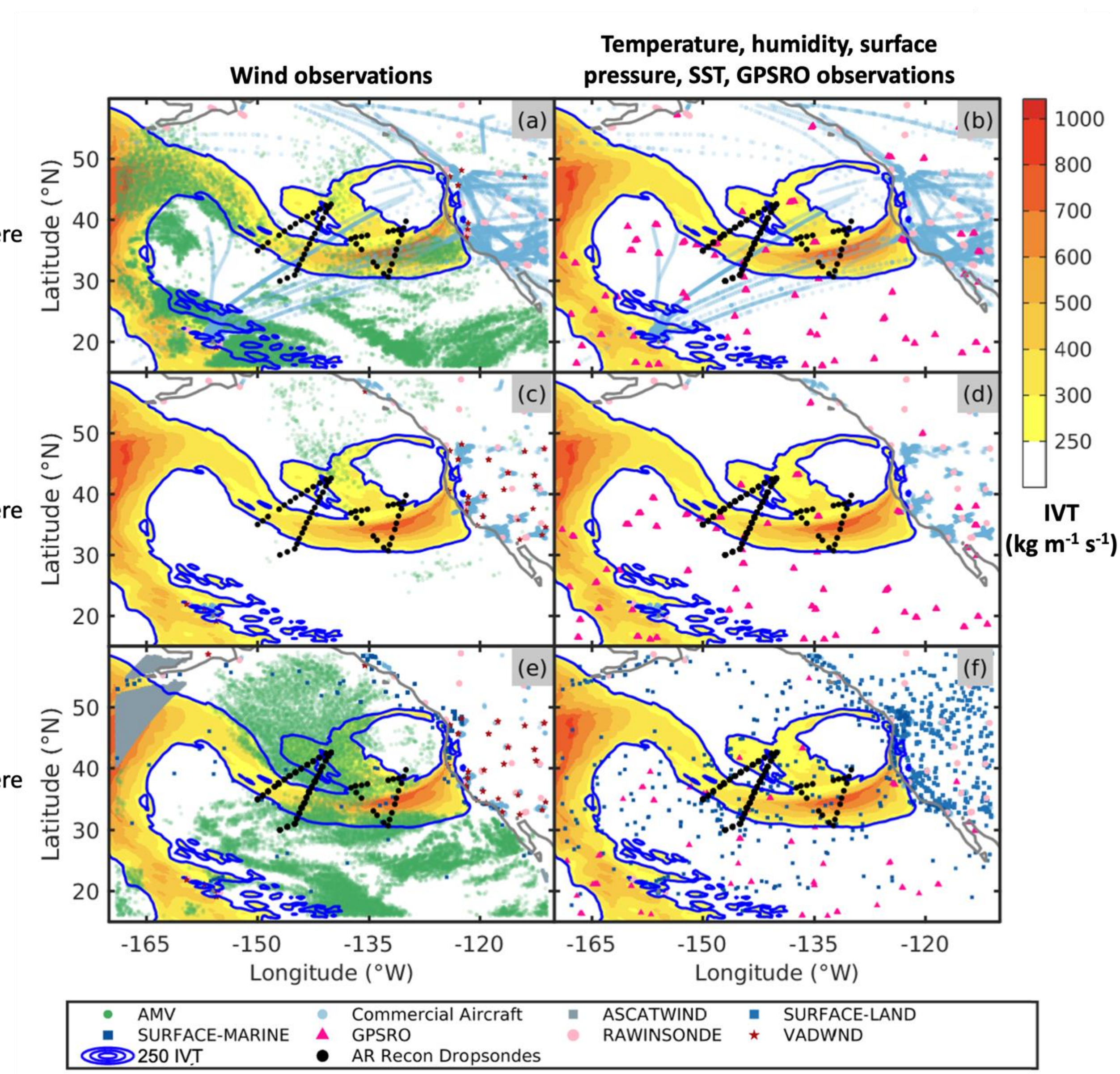

Figure 10. Impact of observations on analysis. The O – B and O – A departures in the ECMWF data assimilation long window shown as grey and cyan dots, respectively, for wind speed, temperature, and specific humidity in BUFR (a-c) and alphanumeric dropsondes (d-f). The O – B and O – A departures averaged in 50-hPa layers are given as solid lines, and the 5th and 95th percentiles of the 50-hPa layers are shown as dashed lines. The number of dropsondes and levels actively assimilated are provided at the top of each panel.

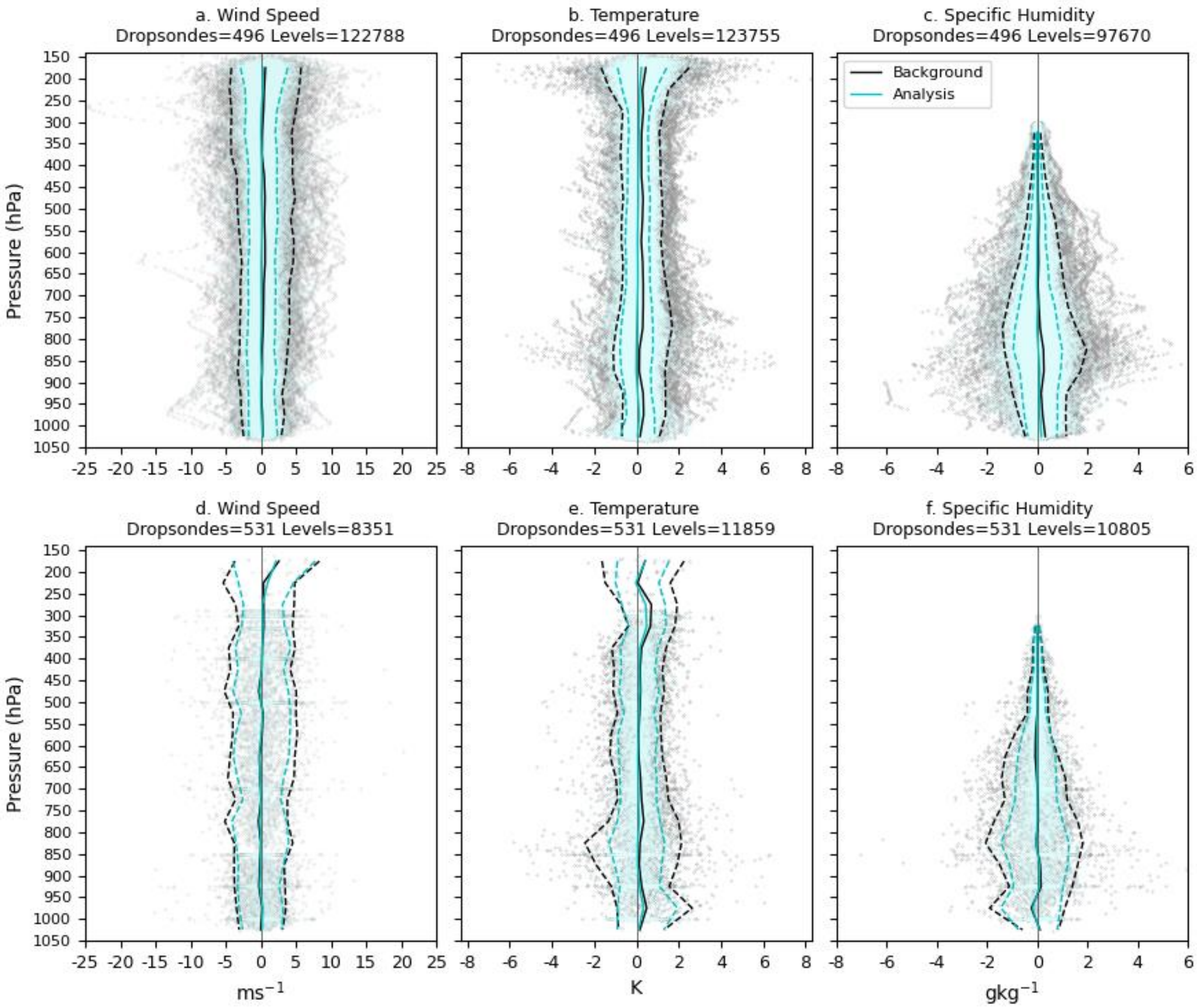

6. Operational challenges

The substantial effort by national and international collaborators resulted in a successful AR Recon season, despite several challenges. Over the course of AR Recon 2021 there were five instances when severe weather conditions impacted the planned C130 flights from Reno. IOPs scheduled for 00 UTC 29th January and 00 UTC 14th February were cancelled due to severe turbulence or cross winds along the route or at departure/arrival times. Flight tracks were modified in IOPs 25, 27, and 28 due to severe turbulence forecast. Weather conditions did not affect the G-IV flight plans, with any significant turbulence below flight level.

For five days in January, the NCEP forecast data was inaccessible to CW3E due to scheduled maintenance and upgrade taking longer than originally planned. During this period, forecasts were made using only the ECMWF data. By using model output from two centers for forecast briefings, AR Recon is building operational resilience to such unforeseeable challenges.

Another unexpected issue occurred in March, when a ruptured water pipe at NWS headquarters interrupted the flow of NOAA National Data Buoy Center (NDBC) data. This did not affect the transmission of data from the AR Recon drifting buoys but did affect the data from moored buoys.

This campaign was completed under COVID-19 restrictions, which represented many operational challenges. This year, less than half of the buoys (30) compared to 2020 (64) were deployed, due to supply restrictions and limited options to distribute via ships of opportunity. Pandemic related restrictions also led to a change of aircraft operations for NOAA and the USAF, as well as the CW3E field team who were responsible for releasing radiosondes.

Several studies have shown the effect of reduced aircraft observations on operational weather forecasting during the pandemic (e.g., Ingleby et al., 2021; James et al., 2020). The WMO Secretariat stated '*it will be crucial to maintain a certain level of investment in core observations that are made for the sole and specific purpose of underpinning the weather, climate, water and environmental services … the crisis has clearly demonstrated the immense value of operational robustness, a quality that is inherent in an observing system consisting of many and diverse* *components operated by a broad group of entities from different sectors and different nations*' (Riishojgaard 2020). AR Recon supports this mission, as a short-term targeted campaign that complements other sources of observational data.

7. Summary

Despite the challenges posed in 2021, the number of observations collected during Atmospheric River Reconnaissance (AR Recon) 2021 far exceeded the number collected during the previous four seasons (Table 2).

AR Recon demonstrates the value of a Research and Operations Partnership (RAOP), with sampling targets based on potential forecast improvement as well as research purposes. Targeted observations were focused on essential atmospheric structures, primarily ARs, but with other meteorological phenomena also considered. Adjoint and ensemble sensitivities, mainly focusing on predictions of U.S. West Coast precipitation, provided complementary information on locations where additional observations may help to constrain the forecast.

The AR Recon data has a wide utility, with dropsonde, buoy and radiosonde data being distributed via the Global Telecommunications System (GTS) in real time for assimilation into numerical weather prediction (NWP) models. This data can also be used for further model diagnostic studies and is also assimilated into reanalysis products. This dataset, along with that not available on the GTS, i.e., ARO and tail radar are valuable for research purposes.

Several studies have demonstrated the positive impact of AR Recon data on NWP forecasts as well as the contribution to understanding ARs and other atmospheric phenomena, and it is hoped that AR Recon will continue to gather these vital observations for future years.

To take advantage of the wide range of collaborators involved in AR Recon as well as the varied expertise of people involved, a case study of sequence 1 (IOPs 3-8) is being organized with contributions from multiple centers. The AR Recon 2021 logo cloud (Figure 11) summarizes the network of collaborators involved across all activities in this successful operational campaign.

*Table 4. Summary of the number of AR Recon observations taken during 2021 compared to previous AR Recon campaigns. *"Operational", National Winter Season Operations Plan (OFCM2019)*

	2021*	**2020***	**2019**	**2018**	**2016**
Number of IOPs	29.5	17	6	6	3
Number of flights	45	31	11	13	6
Dropsondes	1142	738	264	361	270
Radiosondes	111	58	160	191	68
New drifting buoys	30	64	15	-	-
ARO profiles	804	54	0	39	-

Figure 1. AR Recon 2021 logo cloud collaboration diagram. Modeling and DA SC: Modeling and Data Assimilation Steering Committee.

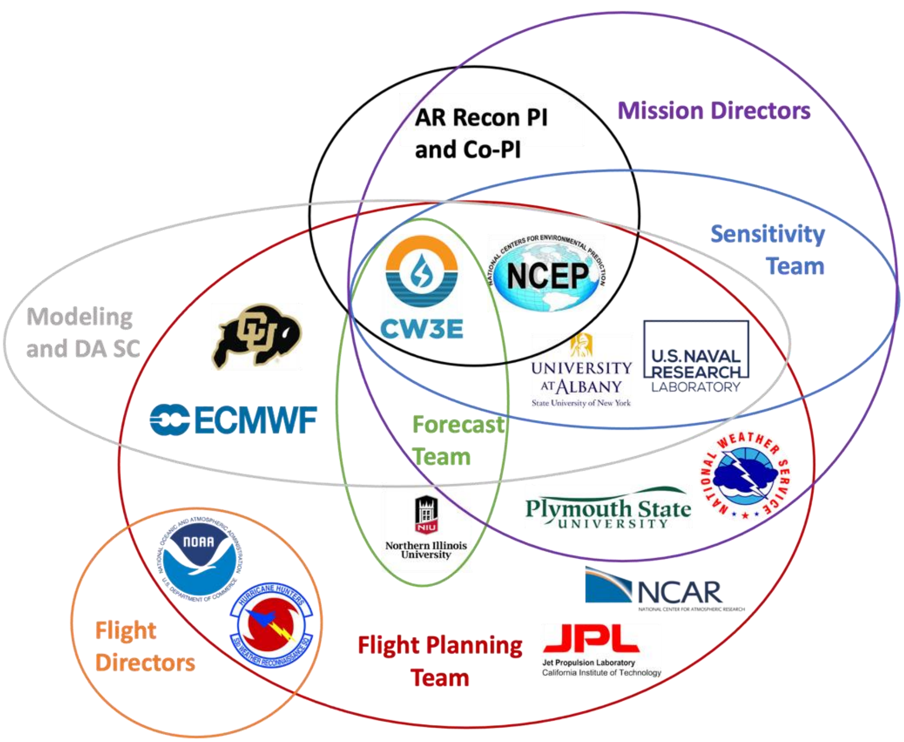

8. Recommendations

For AR Recon 2022, there are plans for the USAF to be on call during 6th to 19th January. Due to operational constraints, AR Recon 2021 did not commence until 13 January (first possible flight 00 UTC 15 January), and so a high impact event that caused a Presidential Disaster Declaration to be issued for the State of Washington (29th December to 16th January) was not sampled. This event was a direct result of a series of ARs, leading to numerous periods of heavy precipitation, with widespread flooding, mudslides, and landslides.

Buoy deployment as part of AR Recon has more than doubled the number of pressure-observing buoys in the northeast Pacific, adding an additional 70 buoys to the 53 non-AR Recon buoys. However, there are an additional 87 buoys within the domain that do not observe sea level pressure. The availability of pressure data in remote oceanic areas has a significant impact on forecast skill (Ingleby and Isaksen 2018), and thus, an increase in participation in the GDP barometer upgrade program is imperative to fill this data gap.

Due to the forecast improvement potential of ARO data (Chen et al. 2018), increasing the density of these observations by utilizing multiple aircraft and disseminating it in real time to the GTS are future objectives, pending upgrades to the communication systems on the aircraft. A positive impact on forecasts has been found with the assimilation of the Constellation Observing System for Meteorology, Ionosphere and Climate-2 (COSMIC-2) Global Navigation Satellite System (GNSS) Radio Occultation (RO) (Lien et al. 2021, Cucurull and Casey 2021), and future work will explore collaborating with COSMIC-II scientists.

In future years it may be possible to explore additional observations, e.g., Airborne EXpendable BathyThermographs (AXBTs) to record ocean temperature as a function of depth, or Air Launched Automonous Micro Observers (ALAMOs) to collect data on ocean temperature, salinity, depth, and circulation. Stepped Frequency Microwave Radiometers (SFMRs) are currently used in operational hurricane reconnaissance (Klotz and Uhlhorn 2014) and provide accurate estimates of surface wind speed. Data from such tools could provide additional insight into air-sea interactions associated with ARs.

In future operational seasons, we aim to consider where upcoming satellite passes intercept potential target regions and therefore more systematically exploit data gaps in our sampling strategy.

The USAF C-130s were based in Reno for most of the season, and the high elevation in particular resulted in difficult flight conditions. The USAF have identified that the base at Mather, CA would be more suitable. Having one aircraft based in Hawaii made it possible to sample systems further west over the Pacific Ocean, with observations collected several days before landfall and enabling longer sequences to be possible, as well as further south to observe interactions between the tropics and mid-latitudes. As many ARs develop in the West Pacific, it may be advantageous to deploy even further west than current operational capabilities, possibly in collaboration with West Pacific campaigns. Looking further ahead, NOAA will transition from the G-IV to the G-550 in winter 2025, with longer range and duration to allow AR Recon to reach farther regions of sensitivity, as well as a much more comprehensive instrument package.

In 2016, observations in the North Atlantic were taken as part of the North Atlantic Waveguide and Downstream Impact Experiment (NAWDEX) (Schäfler et al. 2018), and along with the success of AR Recon in the northeast Pacific, a combined European–American observational campaign in the North Atlantic, 'AR Recon Atlantic' has been proposed (Lavers et al. 2020b). This will make use of the broad experience gained from AR Recon.

On 22nd March 2021, the NCEP GFS model was upgraded (NOAA, 2021) and from AR Recon 2022, it is hoped that GFS will be able to assimilate dropsonde data in BUFR format. Only data from dropsondes deployed by NOAA transmit BUFR data to the GTS in real-time (see Section 5), and a future recommendation is for the upgrade of USAF communications so that they can also transmit these full profile data in real-time, rather than only data on significantly reduced vertical levels.

Data availability statement

ECMWF forecast data are stored in the ECMWF archive: https://www.ecmwf.int/en/forecasts/datasets/archive-datasets

GFS forecast data are downloaded in real time from NCEP NOMADS: https://nomads.ncep.noaa.gov/

NOAA and USAF dropsonde data: https://www.nhc.noaa.gov/recon.php
NOAA data also available at: https://seb.noaa.gov/pub/acdata

Acknowledgements

AR Recon 2021 involved many scientists, engineers, air crews, project managers, program managers, and others. These include individuals from NOAA, NASA, the U.S. Air Force 53rd Weather Reconnaissance Squadron, and elsewhere. Without their efforts, these data would not be available for this study. We also acknowledge Bing Cao, Bruce Ingleby, Luca Centurioni, Allison Michaelis, Adam Sisco for their contributions to AR Recon 2021. Heini Wernli, Maxi Boettcher, and Hanin Binder of ETH Zürich are acknowledged for providing forecasts of warm conveyor belt (WCB) activity.

This research was supported by the California Department of Water Resources AR research program (Award 4600013361) and the U.S. Army Corps of Engineers Engineer Research and Development Center (Awards 609 W912HZ-15-2-0019 and W912HZ-19-2-0023). ARO observations were supported by NSF GRANT AGS-1642650 and AGS-1454125, and NASA GRANT NNX15AU19G. CAR and JDD were supported by the supported by the Chief of Naval Research through the NRL Base Program, PE 0601153N (NRL 6.1 Atmospheric Rivers Project), and used computational resources provided by the Navy DoD Supercomputing Resource Center.

References

American Meteorological Society, 2019: Atmospheric river. Glossary of Meteorology, http://glossary.ametsoc.org/wiki/Atmospheric_river.

Ancell, B. and Hakim, G.J., 2007. Comparing adjoint-and ensemble-sensitivity analysis with applications to observation targeting. Monthly Weather Review, 135(12), pp.4117-4134.

Appenzeller, C.H., Davies, H.C. and Norton, W.A., 1996. Fragmentation of stratospheric intrusions. Journal of Geophysical Research: Atmospheres, 101(D1), pp.1435-1456.

Browning, K.A., 1986. Conceptual models of precipitation systems. Weather and forecasting, 1(1), pp.23-41.

Cardinali, C., Buizza, R., Kelly, G., Shapiro, M. and Thépaut, J.N., 2007. The value of observations. III: Influence of weather regimes on targeting. Quarterly Journal of the Royal Meteorological Society: A journal of the atmospheric sciences, applied meteorology and physical oceanography, 133(628), pp.1833-1842.

Carlson, T.N., 1980. Airflow through midlatitude cyclones and the comma cloud pattern. Monthly Weather Review, 108(10), pp.1498-1509.

Cannon, F., Oakley, N. S., Hecht, C. W., Michaelis, A., Cordeira, J. M., Kawzenuk, B., . . . others (2020). Observations and predictability of a high-impact narrow cold-frontal rainband over southern california on 2 february 2019. Weather and Forecasting, 35 (5), 2083{2097.

Cannon, F., Hecht, C.W., Cordeira, J.M. and Ralph, F.M., 2018. Synoptic and mesoscale forcing of Southern California extreme precipitation. Journal of Geophysical Research: Atmospheres, 123(24), pp.13-714.

Cobb, A., Michaelis, A., Iacobellis, S., Ralph, F., & Delle Monache, L. (2021a). Atmospheric river sectors: Definition and characteristics observed using dropsondes from 2014-2020 CalWater and AR Recon. Monthly Weather Review,1 (aop).

Cobb, A., Delle Monache, L., Cannon, F. and Ralph, F.M., 2021b. Representation of Dropsonde- Observed Atmospheric River Conditions in Reanalyses. Geophysical Research Letters, 48(15), p.e2021GL093357.

Cordeira, J.M., Ralph, F.M., Martin, A., Gaggini, N., Spackman, J.R., Neiman, P.J., Rutz, J.J. and Pierce, R., 2017. Forecasting atmospheric rivers during CalWater 2015. Bulletin of the American Meteorological Society, 98(3), pp.449-459.

Centurioni, L., A. Horányi, C. Cardinali, E. Charpentier, and R. Lumpkin, 2017: A global ocean observing system for measuring sea level atmospheric pressure: effects and impacts on numerical weather prediction. Bull. Amer. Meteor. Soc., 98, 231–238.

Chang, E.K., Zheng, M. and Raeder, K., 2013. Medium-range ensemble sensitivity analysis of two extreme Pacific extratropical cyclones. Monthly weather review, 141(1), pp.211-231.

Chen, X.M., Chen, S.H., Haase, J.S., Murphy, B.J., Wang, K.N., Garrison, J.L., Chen, S.Y., Huang, C.Y., Adhikari, L. and Xie, F., 2018. The impact of airborne radio occultation observations on the simulation of Hurricane Karl (2010). Monthly Weather Review, 146(1), pp.329-350.

Cordeira, J.M., F.M. Ralph,A. Martin, N.Gaggini, J.R. Spackman, P. J. Neiman, J. J. Rutz, and R. Pierce, 2017: Forecasting atmospheric rivers during CalWater 2015. Bull. Amer. Meteor. Soc., 98, 449–459, https://doi.org/10.1175/BAMS-D-15-00245.1.

Cordeira, J.M. and Ralph, F.M., 2021. A Summary of GFS Ensemble Integrated Water Vapor Transport Forecasts and Skill along the US West Coast during Water Years 2017–20. Weather and Forecasting, 36(2), pp.361-377.

Corringham, T. W., F. M. Ralph, A. Gershunov, D. R. Cayan, and C. A. Talbot, 2019: Atmospheric rivers drive flood damages in the western United States. Sci.

Cucurull, L. and Casey, S.P.F., 2021. Improved impacts in observing system simulation experiments of radio occultation observations as a result of model and data assimilation changes. Monthly Weather Review, 149(1), pp.207-220.

Dacre, H.F., Martinez-Alvarado, O. and Mbengue, C.O., 2019. Linking atmospheric rivers and warm conveyor belt airflows. Journal of Hydrometeorology, 20(6), pp.1183-1196.

Demirdjian, R., J. R. Norris, A. Martin, and F. M. Ralph, 2020: Dropsonde observations of the ageostrophy within the pre-coldfrontal low-level jet associated with atmospheric rivers. Mon.Wea.Rev., 148, 1389–1406, https://doi.org/10.1175/MWR-D-19-0248.1.

Dettinger, M.D., Ralph, F.M., Das, T., Neiman, P.J. and Cayan, D.R., 2011. Atmospheric rivers, floods and the water resources of California. Water, 3(2), pp.445-478.

Doyle, J.D., C.A. Reynolds, and C. Amerault, 2019: Adjoint Sensitivity Analysis of High-Impact Extratropical Cyclones. Mon. Wea. Rev., 147, 4511–4532, https://doi.org/10.1175/MWR-D-19-0055.1

Doyle, J.D., C. Amerault, C.A. Reynolds, P. Alex Reinecke, 2014: Initial condition sensitivity and predictability of a severe extratropical cyclone using a moist adjoint. Mon. Wea. Rev., 142, 320-342.

ECMWF, 2020. IFS documentation CY47R1 - Part III: Dynamics and numerical procedures. European Centre for Medium-Range Weather Forecasts. 10.21957/u8ssd58. https://www.ecmwf.int/node/19747

Errico, R. M., 1997: What is an adjoint model? *Bull. Amer. Meteor. Soc.*, **78**, 2577– 2591, https://doi.org/10.1175/1520-0477(1997)078<2577:WIAAM>2.0.CO;2.

Guan, B., Waliser, D.E. and Ralph, F.M., 2018. An intercomparison between reanalysis and dropsonde observations of the total water vapor transport in individual atmospheric rivers. Journal of Hydrometeorology, 19(2), pp.321-337.

Gibson, P.B., Waliser, D.E., Guan, B., DeFlorio, M.J., Ralph, F.M. and Swain, D.L., 2020. Ridging Associated with Drought across the Western and Southwestern United States: Characteristics, Trends, and Predictability Sources. Journal of Climate, 33(7), pp.2485-2508.

Gershunov, A., Shulgina, T., Ralph, F.M., Lavers, D.A. and Rutz, J.J., 2017. Assessing the climate- scale variability of atmospheric rivers affecting western North America. Geophysical Research Letters, 44(15), pp.7900-7908.

National Drought Mitigation Center, 2021. U.S. Drought Monitor, https://droughtmonitor.unl.edu/

Grams, C.M., Wernli, H., Böttcher, M., Čampa, J., Corsmeier, U., Jones, S.C., Keller, J.H., Lenz, C.J. and Wiegand, L., 2011. The key role of diabatic processes in modifying the upper-tropospheric wave guide: a North Atlantic case- study. Quarterly Journal of the Royal Meteorological Society, 137(661), pp.2174-2193.

Haase, J. S., M. J. Murphy, Jr., B. Cao, F. M. Ralph, M. Zheng, and L. Delle Monache (2021), Multi-GNSS Airborne Radio Occultation Observations as a Complement to Dropsondes in Atmospheric River Reconnaissance, *J. Geophys. Res.-Atmos.*, *Submitted*.

Haase, J. S., B. J. Murphy, P. Muradyan, F. Nievinski, K. M. Larson, J. L. Garrison, and K.-N. Wang (2014), First Results from an Airborne GPS Radio Occultation System for Atmospheric Profiling, *Geophysical Research Letters*, *41*, 1759-1765.

Henn, B., Musselman, K.N., Lestak, L., Ralph, F.M. and Molotch, N.P., 2020. Extreme runoff generation from atmospheric river driven snowmelt during the 2017 Oroville Dam spillways incident. Geophysical Research Letters, 47(14), p.e2020GL088189.

Hill, A.J., Weiss, C.C. and Ancell, B.C., 2020. Factors Influencing Ensemble Sensitivity–Based Targeted Observing Predictions at Convection-Allowing Resolutions. Monthly Weather Review, 148(11), pp.4497-4517.

Hobbs, P.V. and Persson, P.O.G., 1982. The mesoscale and microscale structure and organization of clouds and precipitation in midlatitude cyclones. Part V: The substructure of narrow cold-frontal rainbands. Journal of Atmospheric Sciences, 39(2), pp.280-295.

Hobbs, P.V., 1978. Organization and structure of clouds and precipitation on the mesoscale and microscale in cyclonic storms. Reviews of Geophysics, 16(4), pp.741-755.

Hodur, R. M., 1997: The Naval Research Laboratory’s Coupled Ocean/Atmosphere Mesoscale Prediction System (COAMPS). Mon. Wea. Rev., 125, 1414–1430, https://doi.org/10.1175/1520-0493(1997)125,1414:TNRLSC.2.0.CO;2.

Horányi, A., Cardinali, C. and Centurioni, L., 2017. The global numerical weather prediction impact of mean- sea- level pressure observations from drifting buoys. Quarterly Journal of the Royal Meteorological Society, 143(703), pp.974-985.

Hoskins, B.J., McIntyre, M.E. and Robertson, A.W., 1985. On the use and significance of isentropic potential vorticity maps. Quarterly Journal of the Royal Meteorological Society, 111(470), pp.877-946.

Ingleby, B. and L. Isaksen, 2018: Drifting buoy pressures: impact on NWP. Atmos. Sci. Lett., 19:e822

Ingleby, B., Candy, B., Eyre, J., Haiden, T., Hill, C., Isaksen, L., Kleist, D., Smith, F., Steinle, P., Taylor, S. and Tennant, W., 2021. The Impact of COVID- 19 on weather forecasts: a balanced view. Geophysical research letters, 48(4), p.e2020GL090699.

James, E.P., Benjamin, S.G. and Jamison, B.D., 2020. Commercial-Aircraft-Based Observations for NWP: Global Coverage, Data Impacts, and COVID-19. Journal of Applied Meteorology and Climatology, 59(11), pp.1809-1825.

Jasperse, J., Ralph, F.M., Anderson, M., Brekke, L., Malasavage, N., Dettinger, M.D., Forbis, J., Fuller, J., Talbot, C., Webb, R. and Haynes, A., 2020. Lake Mendocino Forecast Informed Reservoir Operations Final Viability Assessment.

Jorgensen, D.P., Pu, Z., Persson, P.O.G. and Tao, W.K., 2003. Variations associated with cores and gaps of a Pacific narrow cold frontal rainband. Monthly weather review, 131(11), pp.2705-2729.

Kamae, Y., Mei, W., Xie, S.P., Naoi, M. and Ueda, H., 2017. Atmospheric rivers over the northwestern Pacific: Climatology and interannual variability. Journal of Climate, 30(15), pp.5605-5619.

Klotz, B.W. and Uhlhorn, E.W., 2014. Improved stepped frequency microwave radiometer tropical cyclone surface winds in heavy precipitation. Journal of Atmospheric and Oceanic Technology, 31(11), pp.2392-2408.

Lavers, D.A., Allan, R.P., Wood, E.F., Villarini, G., Brayshaw, D.J. and Wade, A.J., 2011. Winter floods in Britain are connected to atmospheric rivers. Geophysical Research Letters, 38(23).

Lavers, M. J. Rodwell, D. S. Richardson, F. M. Ralph, J. D. Doyle, C. A. Reynolds, V. Tallapragada, and F. Pappenberger, 2018: The gauging and modeling of rivers in the sky. Geophys. Res. Lett., 45, 7828–7834, https://doi.org/10.1029/2018GL079019.

Lavers, D.A., Ingleby, N.B., Subramanian, A.C., Richardson, D.S., Ralph, F.M., Doyle, J.D., Reynolds, C.A., Torn, R.D., Rodwell, M.J., Tallapragada, V. and Pappenberger, F., 2020a. Forecast errors and uncertainties in Atmospheric Rivers. Weather and Forecasting, 35(4), pp.1447-1458.

Lavers, D.A., Ralph, F.M., Richardson, D.S. and Pappenberger, F., 2020b. Improved forecasts of atmospheric rivers through systematic reconnaissance, better modelling, and insights on conversion of rain to flooding. Communications Earth & Environment, 1(1), pp.1-7.

Lavers, D. A, Ingleby, B., Centurioni, L., Wilson, A.M., Ralph, F.M., Subramanian, A, 2020c. Drifting buoys deployed in the northeast Pacific. ECMWF Newsletter 163. https://www.ecmwf.int/en/newsletter/163/news/drifting-buoys-deployed-northeast-pacific

Lien, G.Y., Lin, C.H., Huang, Z.M., Teng, W.H., Chen, J.H., Lin, C.C., Ho, H.H., Huang, J.Y., Hong, J.S., Cheng, C.P. and Huang, C.Y., 2021. Assimilation Impact of Early FORMOSAT-7/COSMIC-2 GNSS Radio Occultation Data with Taiwan's CWB Global Forecast System. Monthly Weather Review.

Madonna, E., Wernli, H., Joos, H. and Martius, O., 2014a. Warm conveyor belts in the ERA-Interim dataset (1979–2010). Part I: Climatology and potential vorticity evolution. Journal of Climate, 27(1), pp.3-26.

Madonna, E., Limbach, S., Aebi, C., Joos, H., Wernli, H. and Martius, O., 2014b. On the co-occurrence of warm conveyor belt outflows and PV streamers. Journal of the atmospheric sciences, 71(10), pp.3668-3673.

Majumdar, S.J., 2016. A review of targeted observations. Bulletin of the American Meteorological Society, 97(12), pp.2287-2303.

Martin, A.C., Ralph, F.M., Wilson, A., DeHaan, L. and Kawzenuk, B., 2019. Rapid cyclogenesis from a mesoscale frontal wave on an atmospheric river: Impacts on forecast skill and predictability during atmospheric river landfall. Journal of Hydrometeorology, 20(9), pp.1779-1794.

Massacand, A.C., Wernli, H. and Davies, H.C., 1998. Heavy precipitation on the Alpine southside: An upper- level precursor. Geophysical Research Letters, 25(9), pp.1435-1438.

Martius, O., Zenklusen, E., Schwierz, C. and Davies, H.C., 2006. Episodes of Alpine heavy precipitation with an overlying elongated stratospheric intrusion: A climatology. International Journal of Climatology: A Journal of the Royal Meteorological Society, 26(9), pp.1149-1164.

Martius, O., Sodemann, H., Joos, H., Pfahl, S., Winschall, A., Croci- Maspoli, M., Graf, M., Madonna, E., Mueller, B., Schemm, S. and Sedláček, J., 2013. The role of upper- level dynamics and surface processes for the Pakistan flood of July 2010. Quarterly Journal of the Royal Meteorological Society, 139(676), pp.1780-1797.

Mundhenk, B.D., Barnes, E.A. and Maloney, E.D., 2016. All-season climatology and variability of atmospheric river frequencies over the North Pacific. Journal of Climate, 29(13), pp.4885-4903.

Neiman, P.J., Gaggini, N., Fairall, C.W., Aikins, J., Spackman, J.R., Leung, L.R., Fan, J., Hardin, J., Nalli, N.R. and White, A.B., 2017. An analysis of coordinated observations from NOAA's Ronald H. Brown ship and G-IV aircraft in a landfalling atmospheric river over the North Pacific during CalWater-2015. Monthly weather review, 145(9), pp.3647-3669.

Neiman, P.J., Wick, G.A., Moore, B.J., Ralph, F.M., Spackman, J.R. and Ward, B., 2014. An airborne study of an atmospheric river over the subtropical Pacific during WISPAR: Dropsonde budget-box diagnostics and precipitation impacts in Hawaii. Monthly weather review, 142(9), pp.3199-3223.

NOAA (2021). NOAA upgrades flagship U.S. global weather model. https://www.noaa.gov/media-release/noaa-upgrades-flagship-us-global-weather-model

Norris, J.R., F.M. Ralph, R. Demirdjian, F. Cannon, B. Blomquist, C.W. Fairall, J.R. Spackman, S. Tanelli, and D.E. Waliser, 2020: The Observed Water Vapor Budget in an Atmospheric River over the Northeast Pacific. J. Hydrometeor., 21, 2655–2673, https://doi.org/10.1175/JHM-D-20-0048.1

Oakley, N.S., Lancaster, J.T., Kaplan, M.L. and Ralph, F.M., 2017. Synoptic conditions associated with cool season post-fire debris flows in the Transverse Ranges of southern California. Natural Hazards, 88(1), pp.327-354.

OFCM, 2019: National Winter Season Operations Plan (NWSOP). Office of the Federal Coordinator for Meteorological Services and Supporting Research, 84 pp., www.ofcm.gov/publications/nwsop/2019_nwsop.pdf

Predictive Services National Interagency Fire Center (2021). National Significant Wildland Fire Potential Outlook. https://www.predictiveservices.nifc.gov/outlooks/monthly_seasonal_outlook.pdf

Rabier, F., Klinker, E., Courtier, P. and Hollingsworth, A., 1996. Sensitivity of forecast errors to initial conditions. Quarterly Journal of the Royal Meteorological Society, 122(529), pp.121-150.

Ralph, F.M., Neiman, P.J., Wick, G.A., Gutman, S.I., Dettinger, M.D., Cayan, D.R. and White, A.B., 2006. Flooding on California's Russian River: Role of atmospheric rivers. Geophysical Research Letters, 33(13).

Ralph, F.M., Prather, K.A., Cayan, D., Spackman, J.R., DeMott, P., Dettinger, M., Fairall, C., Leung, R., Rosenfeld, D., Rutledge, S. and Waliser, D., 2016. CalWater field studies designed to quantify the roles of atmospheric rivers and aerosols in modulating US West Coast precipitation in a changing climate. Bulletin of the American Meteorological Society, 97(7), pp.1209-1228.

Ralph, F.M., Dettinger, M., Lavers, D., Gorodetskaya, I.V., Martin, A., Viale, M., White, A.B., Oakley, N., Rutz, J., Spackman, J.R. and Wernli, H., 2017. Atmospheric rivers emerge as a global science and applications focus. Bulletin of the American Meteorological Society, 98(9), pp.1969-1973.

Ralph, F.M., Rutz, J.J., Cordeira, J.M., Dettinger, M., Anderson, M., Reynolds, D., Schick, L.J. and Smallcomb, C., 2019. A scale to characterize the strength and impacts of atmospheric rivers. Bulletin of the American Meteorological Society, 100(2), pp.269-289.

Ralph, F.M., F. Cannon, V. Tallapragada, C.A. Davis, J.D. Doyle, F. Pappenberger, A. Subramanian, A.M. Wilson, D.A. Lavers, C.A. Reynolds, J.S. Haase, L. Centurioni, B. Ingleby, J.J. Rutz, J.M. Cordeira, M. Zheng, C. Hecht, B. Kawzenuk, and L. Delle Monache, 2020: West Coast Forecast Challenges and Development of Atmospheric River Reconnaissance. Bull. Amer. Meteor. Soc., 101(8), E1357–E1377, https://doi.org/10.1175/BAMS-D-19-0183.1

Ralph, F.M., Woodside, G., Anderson, M., Cleary-Rose, K., Haynes, A., Jasperse, J., Sweeten, J., Talbot, C., Tyler, J. and Vermeeren, R., 2021. Prado Dam Forecast Informed Reservoir Operations Preliminary Viability Assessment.

Reynolds, C.A., Doyle, J.D., Ralph, F.M. and Demirdjian, R., 2019. Adjoint sensitivity of North Pacific atmospheric river forecasts. Monthly Weather Review, 147(6), pp.1871-1897.

Reynolds, C.A., Doyle, J.D., Hodur, R.M. and Jin, H., 2010. Naval Research Laboratory multiscale targeting guidance for T-PARC and TCS-08. Weather and forecasting, 25(2), pp.526-544.

Riishojgaard, 2020: Impacts of COVID-19 Restrictions on Observations and Monitoring, Bulletin nº : Vol 69 (2) (https://public.wmo.int/en/resources/bulletin/impacts-of-covid-19-restrictions-observations-and-monitoring)

Rodwell, M., Forbes, R. and Wernli, H., 2018. Why warm conveyor belts matter in NWP. ECMWF Newsletter, 154, pp.21-28.

Ruston, B. and Healy, S., 2021. Forecast Impact of FORMOSAT- 7/COSMIC- 2 GNSS Radio Occultation Measurements. Atmospheric Science Letters, 22(3), p.e1019.

Sanders, F. and Gyakum, J.R., 1980. Synoptic-dynamic climatology of the “bomb”. Monthly Weather Review, 108(10), pp.1589-1606.

Ryoo, J.M., Kaspi, Y., Waugh, D.W., Kiladis, G.N., Waliser, D.E., Fetzer, E.J. and Kim, J., 2013. Impact of Rossby wave breaking on US West Coast winter precipitation during ENSO events. Journal of Climate, 26(17), pp.6360-6382.

Schmit, T.J., Griffith, P., Gunshor, M.M., Daniels, J.M., Goodman, S.J. and Lebair, W.J., 2017. A closer look at the ABI on the GOES-R series. Bulletin of the American Meteorological Society, 98(4), pp.681-698.

Schreiner, W.S., Weiss, J.P., Anthes, R.A., Braun, J., Chu, V., Fong, J., Hunt, D., Kuo, Y.H., Meehan, T., Serafino, W. and Sjoberg, J., 2020. COSMIC- 2 radio occultation constellation: First results. Geophysical Research Letters, 47(4), p.e2019GL086841.

Schäfler, A., Craig, G., Wernli, H., Arbogast, P., Doyle, J.D., McTaggart-Cowan, R., Methven, J., Rivière, G., Ament, F., Boettcher, M. and Bramberger, M., 2018. The North Atlantic waveguide and downstream impact experiment. Bulletin of the American Meteorological Society, 99(8), pp.1607-1637.

Stone, R.E., Reynolds, C.A., Doyle, J.D., Langland, R.H., Baker, N.L., Lavers, D.A. and Ralph, F.M., 2020. Atmospheric river reconnaissance observation impact in the Navy global forecast system. Monthly Weather Review, 148(2), pp.763-782.

Stull, R.B., 1985. Predictability and scales of motion. Bulletin of the American Meteorological Society, 66(4), pp.432-436.

Sprenger, M. and Wernli, H., 2015. The LAGRANTO Lagrangian analysis tool–version 2.0. Geoscientific Model Development, 8(8), pp.2569-2586.

Subramanian 2021. The Impact of Oceanic Buoys with Surface Pressure on Forecasts in Winter 2019 and 2020

Sukup, S. J., J. Laber, D. Sweet, and R. Thompson, 2015: Analysis of an intense narrow cold frontal rainband and the Springs Fire burn area debris flow of 12 December 2014. NWS Tech. Attachment 1601, 32 pp., http://www.wrh.noaa.gov/media/wrh/online_publications/TAs/TA1601.pdf.

Tallapragada, V., Stephen J. Lord, Xingren Wu and F. Martin Ralph, 2021: Forecast Impacts of the Dropwindsonde Observations on the NCEP Global Forecast System during the 2020 Atmospheric Rivers Observing Campaign. (To be submitted to Weather and Forecasting).

Torn, R. D., and G. J. Hakim, 2008: Ensemble-based sensitivity analysis. *Mon. Wea. Rev.*, **136**, 663–677, https://doi.org/10.1175/2007MWR2132.1.

Torn, R.D. and Hakim, G.J., 2009. Initial condition sensitivity of western Pacific extratropical transitions determined using ensemble-based sensitivity analysis. Monthly weather review, 137(10), pp.3388-3406.

Torn, R.D., 2014. The impact of targeted dropwindsonde observations on tropical cyclone intensity forecasts of four weak systems during PREDICT. Monthly Weather Review, 142(8), pp.2860-2878.

Uccellini, L.W., Keyser, D., Brill, K.F. and Wash, C.H., 1985. The Presidents' Day cyclone of 18–19 February 1979: Influence of upstream trough amplification and associated tropopause folding on rapid cyclogenesis. Monthly Weather Review, 113(6), pp.962-988.

Waliser, D. and Guan, B., 2017. Extreme winds and precipitation during landfall of atmospheric rivers. Nature Geoscience, 10(3), pp.179-183.

Wang, C.C. and Rogers, J.C., 2001. A composite study of explosive cyclogenesis in different sectors of the North Atlantic. Part I: Cyclone structure and evolution. Monthly Weather Review, 129(6), pp.1481-1499.

Wash, C.H., Peak, J.E., Calland, W.E. and Cook, W.A., 1988. Diagnostic study of explosive cyclogenesis during FGGE. Monthly Weather Review, 116(2), pp.431-451.

Wernli, B.H. and Davies, H.C., 1997. A Lagrangian- based analysis of extratropical cyclones. I: The method and some applications. Quarterly Journal of the Royal Meteorological Society, 123(538), pp.467-489.

Wernli, H. and Sprenger, M., 2007. Identification and ERA-15 climatology of potential vorticity streamers and cutoffs near the extratropical tropopause. Journal of the atmospheric sciences, 64(5), pp.1569-1586.

Yoshida, A. and Asuma, Y., 2004. Structures and environment of explosively developing extratropical cyclones in the northwestern Pacific region. Monthly Weather Review, 132(5), pp.1121-1142.

Žagar, N., Horvat, M., Zaplotnik, Ž. and Magnusson, L., 2017. Scale-dependent estimates of the growth of forecast uncertainties in a global prediction system. Tellus A: Dynamic Meteorology and Oceanography, 69(1), p.1287492.

Zhang, S., Fu, G., Lu, C. and Liu, J., 2017. Characteristics of explosive cyclones over the Northern Pacific. Journal of Applied Meteorology and Climatology, 56(12), pp.3187-3210.

Zhang, Z., Ralph, F.M. and Zheng, M., 2019. The relationship between extratropical cyclone strength and atmospheric river intensity and position. Geophysical Research Letters, 46(3), pp.1814-1823.

Zhang, Z. and Ralph, F.M., 2021. The Influence of Antecedent Atmospheric River Conditions on Extratropical Cyclogenesis. Monthly Weather Review, 149(5), pp.1337-1357.

Zheng, M., Delle Monache, L., Wu, X., Ralph, F.M., Cornuelle, B., Tallapragada, V., Haase, J.S., Wilson, A.M., Mazloff, M., Subramanian, A. and Cannon, F., 2021a. Data gaps within atmospheric rivers over the northeastern Pacific. Bulletin of the American Meteorological Society, 102(3), pp.E492-E524.

Zheng, M., Delle Monache, L., Cornuelle, B. D., Ralph, F. M., Tallapragada, V. S., Subramanian, A., Haase, J. S., Zhang, Z., Wu, X., Murphy, M. J., Higgins, T. B., and DeHaan, L., 2021b. Improved forecast skill through assimilating dropsonde observations from Atmospheric River Reconnaissance. *Journal of Geophysical Research - Atmosphere, under review.*

Zheng, M., Chang, E.K. and Colle, B.A., 2013. Ensemble sensitivity tools for assessing extratropical cyclone intensity and track predictability. Weather and forecasting, 28(5), pp.1133-1156.

Zhu, Y. and Newell, R.E., 1998. A proposed algorithm for moisture fluxes from atmospheric rivers. Monthly weather review, 126(3), pp.725-735.

Zhu, Y., Liu, E., Mahajan, R., Thomas, C., Groff, D., Van Delst, P., Collard, A., Kleist, D., Treadon, R. and Derber, J.C., 2016. All-sky microwave radiance assimilation in NCEP's GSI analysis system. Monthly Weather Review, 144(12), pp.4709-4735.

Supplementary

Click here to access/download
Supplemental Material
Supplementary Material.docx